IgG3 Hinge Architecture Expands Dengue Virus Breadth of A Quaternary Epitope Dependent Zika Virus Cross-Neutralizing Antibody

Sanjeev Kumar[1,2,3,4,†,*], Connor A. P. Scott[5,6,†], Lingling Xu[1,2,3,†], Kathryn Moore[1,2,3,7], Jacob V. Velden[1,2,3,7], Samuel Shih[1,2,3], Richard H. West[1,2,3], Sneh Lata Gupta[1,2,3], Naphak Modhiran[5,6], Mehul S. Suthar[1,2,3,7,8], Daniel Watterson[5,6,*], Jens Wrammert[1,2,3,*]

[1]Division of Infectious Diseases, Department of Pediatrics, School of Medicine, Emory University, Atlanta, GA, USA

[2]Emory Vaccine Center, Emory University School of Medicine, Atlanta, GA, USA

[3]Centers for Childhood Infections and Vaccines, Children's Healthcare of Atlanta, Emory University, Department of Pediatrics, Department of Medicine, Atlanta, GA, USA

[4]ICGEB-Emory Vaccine Program, International Centre for Genetic Engineering and Biotechnology, New Delhi, India

[5]School of Chemistry and Molecular Biosciences, The University of Queensland St Lucia, Brisbane, Australia

[6]Australian Infectious Diseases Research Centre, Brisbane, Australia

[7]Emory National Primate Research Center, Atlanta, GA, USA

[8]Department of Microbiology and Immunology, Emory University, Atlanta, GA, USA

[†]These authors contributed equally to this work

[*]Co-corresponding authors: Sanjeev Kumar (sanjeev@icgeb.res.in); Daniel Watterson (d.watterson@uq.edu.au); Jens Wrammert (jwramme@emory.edu)

Keywords

DENV, ZIKV, neutralizing antibody, IgG3 subclass, cryo-EM, Flaviviruses

ABSTRACT

Defining how antibodies achieve broad neutralization across antigenically related flaviviruses is essential for rational therapeutics and vaccine design. Here, we describe 3A06, a human monoclonal antibody that neutralizes dengue virus (DENV) serotypes 1-3 and zika virus (ZIKV). Notably, subclass switching to IgG3 exhibits expanded neutralizing activity against all four DENV serotypes. High-resolution cryo-electron microscopy (cryo-EM) analysis of 3A06 Fab bound to chimeric ZIKV virions shows that 3A06 engages a quaternary epitope spanning three E protomers. Functional analyses identify a major functional contribution from the light-chain, where somatic hypermutations are critical for neutralization potency, and reversion of improbable mutations substantially reduces neutralization and increases antibody dependent enhancement (ADE) at sub-neutralizing concentrations. Cryo-EM analyses of intact IgG3 in complex with chimeric DENV2 and DENV4 show that the conformational flexibility and extended IgG3 Fc-hinge enable bivalent engagement across E-protein rafts in multiple configurations, overcoming geometrical constraints that limit binding in the IgG1 format. Together, these results define a distinct mode of epitope recognition relative to previously characterized E-dimer epitope (EDE)-specific broadly neutralizing antibodies (bnAbs), and demonstrate how IgG3 subclass architecture can expand virus neutralization breadth. These insights inform the rational engineering of antibodies and vaccines targeting quaternary epitopes on flaviviruses to overcome viral diversity.

42 **INTRODUCTION**

43 Flaviviruses such as dengue virus (DENV) and Zika virus (ZIKV) impose a significant
44 global health burden, with over 400 million infections annually, yet effective strategies for
45 achieving broad and safe vaccines or therapeutics remain limited [1,2]. Antibody-mediated
46 protection is central to vaccine and therapeutic strategies, but is constrained by serotype
47 specificity and the potential risk of antibody-dependent enhancement (ADE) [3,4]. The envelope
48 (E) glycoprotein of flaviviruses, which mediates viral entry, is a major target of neutralizing
49 antibodies (nAbs) [3,5–7]. While monomeric E protein has often been used in vaccines and
50 diagnostics, recent studies suggest that E protein dimers, which are present as quaternary
51 structure on mature flavivirus virions, represent promising templates for rational vaccine design
52 [3,4,8,9].

53 The E protein of flaviviruses exists in different conformational states during the viral life
54 cycle, including a trimeric state together with the virally encoded pr chaperone in immature viral
55 particles and as E dimers which assemble into the rafts of the mature infectious virions [10,11]. The
56 majority of the existing neutralizing monoclonal antibodies (mAbs) recognize epitopes on the
57 monomeric form of E protein targeting its fusion loop epitope (FLE) or EDIII domain [12]. However,
58 a few antibodies that selectively engage the so called envelope dimer epitopes (EDE) formed on
59 the dimeric form of E protein, in the context of the pre-fusion conformation on mature virions,
60 have recently been described [5,6,13–18]. Antibodies capable of binding such quaternary epitopes
61 have shown increased breadth and potency in recent studies, suggesting that targeting of dimeric
62 E-protein conformation on the viral surface is a possible approach for designing broad flavivirus
63 vaccines and therapeutics [5,14,15]. The quaternary epitopes targeted on the E-protein are known
64 to mediate broad DENV neutralization. However, it remains unclear how antibody intrinsic

65 features, and IgG subclass architecture, govern epitope recognition, breadth, and enhancement
66 risk.

67 We previously identified several DENV and ZIKV nAbs from the plasmablasts of DENV2
68 infected donors. One of those nAbs 33.3A06 (described as 3A06 throughout this study) showed
69 potent ZIKV neutralization despite being isolated from a DENV2 infected donor [7,12]. In this study,
70 we carried out a detailed characterization of 3A06 and found that it recognizes a quaternary
71 epitope spanning multiple E protein protomers, with no detectable binding to soluble E
72 monomers. Cryo-electron microscopy analysis of the 3A06 Fab in complex with chimeric ZIKV
73 particles confirmed this mode of recognition. Functional studies further showed that somatic
74 hypermutations in the light chain make a major contribution to neutralization potency. We also
75 found that antibody subclass influences neutralization breadth. When expressed as IgG3, 3A06
76 gained the ability to neutralize all four DENV serotypes, whereas the IgG1 form did not neutralize
77 DENV4. Structural analysis of intact IgG3 in complex with DENV2 and DENV4 particles showed
78 that the extended hinge region supports bivalent engagement of the virion surface, providing a
79 structural basis for the broader activity observed in this subclass. Together, these findings
80 provide insight into antibody recognition of flaviviruses and inform approaches for antibody
81 design and vaccine development.

82 **RESULTS**

83 **3A06 antibody recognizes a quaternary E-protein dimer epitope**

84 We previously reported the discovery of a fully human monoclonal antibody (mAb) 3A06
85 from the plasmablasts of a DENV2 infected donor[7,12]. The 3A06 mAb neutralized ZIKV more
86 potently than DENV1-3 serotypes with up to 45-fold difference in potency, despite being
87 originally isolated from a DENV2 infected donor. To understand the epitope specificity, we first
88 assessed its binding profile using ELISA and biolayer interferometry. The 3A06 mAb binds to
89 recombinant soluble E (sE) protein dimers captured on Streptactin-XT coated plates that were
90 derived from DENV1-3 and ZIKV, but fail to engage DENV4 dimers. The antibody showed little or
91 no detectable binding to sE monomers, the EDIII domain or to viral lysates (**Figures 1A and S1A-**
92 **D**). Using a live virus-based focus reduction neutralization test (FRNT) assay, we observed that
93 3A06 neutralized DENV1-3 with $FRNT_{50}$ values of 0.07 – 0.1 μg/ml. This is comparable to EDE1-
94 C10 (0.3 – 0.6 μg/ml) and EDE2-A11 (0.6 μg/ml) mAbs, while modestly lower against ZIKV as
95 compared to EDE1-C10 (**Figure 1B**). Biolayer interferometry (BLI) analysis revealed a
96 heterogenous interaction of 3A06 in the micromolar (2.62 μM) to picomolar (1.78 pM) range
97 against DENV and ZIKV E-protein dimers (**Figure 1C**). Together, these findings establish that
98 3A06 recognizes a quaternary epitope associated with multiple E-proteins.

99 **Cryo-EM structure of 3A06 reveals recognition of a quaternary epitope spanning multiple**
100 **E protomers**

101 To understand the molecular basis of differences observed in 3A06 binding and
102 neutralization against DENV and ZIKV, we first determined the structure of 3A06 Fab in complex
103 with chimeric ZIKV virions. Here, we used the Binjari virus (BinJV) chimeric system [19–21], an
104 insect-specific flavivirus, which has been shown to reproduce key structural and antigenic
105 features of pathogenic flaviviruses while maintaining a high safety profile. The ZIKV structural

106 proteins were presented on a Binjari virus backbone (herein bZIKV), to generate chimeric virions
107 suitable for high-resolution cryo-EM analysis of 3A06 Fab binding. The 4.6 Å cryo-EM structure
108 of bZIKV complexed with 3A06 Fab at 4°C showed that 3A06 binds a quaternary E-protein
109 dependent epitope across three E protomers with 120 Fab fragments visible on the surface of
110 the virion (**Figure 2A, Figure S2 and Table S1**). This structure was further refined using
111 symmetry expansion of the asymmetric unit to produce a 3.1 Å map that could then be modelled
112 (**Figure 2B**). The atomic model of bZIKV complexed with 3A06 Fab further highlighted the
113 quaternary nature of the 3A06 epitope, showing extensive hydrogen bonding across three E
114 protomers per Fab fragment (**Figure 2C**). Within the asymmetric unit, two 3A06 Fabs bind at the
115 2- and 3- fold axis respectively (**Figure 2C**). Each Fab binds across EDI and EDIII of one E
116 protomer, and EDII of the neighboring two protomers, forming multiple bonds between the Fab
117 and bZIKV (**Figure 3A, and 3B**). The VH of 3A06 buries 875 $Å^2$ across two E protomers making
118 six hydrogen bonds between its complementarity-determining region 2 (HCDR2) and HCDR3
119 loops and EDII of one E protomer and one hydrogen bond across to the neighboring EDI. R109
120 in the HCDR3 loop forms a salt bridge with D71 in the bZIKV bc loop, a highly conserved residue
121 between ZIKV, and DENV serotypes 1-3 (**Figure 2C, 3B, 3C and Figures S3-S5**). Notably, DENV4
122 contains an alanine at position 71, which likely reduces the interaction strength of the 3A06 VH
123 to DENV-4. The VL of 3A06 buries 673 $Å^2$ with extensive hydrogen bonds between LCDR2 and
124 EDIII and EDI of one E protomer, LCDR1 and the fusion loop and bc loop of the neighboring E
125 protomer, and LCDR3 and the hi loop of the third E protomer (**Figure 2C, 3B and 3C**).
126 Interestingly, several key hydrogen bonds for 3A06 to bZIKV were identified as low frequency
127 mutations (2-10%) in germline mutation probability analysis (**Figure S6A, B**). S53, in the CDR-
128 2 loop of 3A06 VL, which forms a hydrogen bond with K373 on EDIII of bZIKV E protomer A, and
129 N33 which interacts with G104 of the E protomer C fusion loop. While G104 is highly conserved
130 across flaviviruses, K373 is not conserved among DENV serotypes and ZIKV, with DENV1, 2, and

131 3 having a proline, and DENV4 having a valine at the equivalent position (**Figure 3B and Figures**
132 **S3-S5**). Overall sequence conservation of the 3A06 epitope shows that the residues on EDII,
133 including the FL, hi, and bc loop contacted by the VH and VL are more conserved between DENV1-
134 4 and ZIKV compared to the quaternary contacts facilitated by the light chain primarily on EDI
135 and EDIII (**Figure S3 and Figures S3-S5**). These contacts suggest that the VL interactions
136 contribute substantially to the stabilization and recognition of the 3A06 epitope on ZIKV.
137 Further, the structure provides insights into the quaternary epitope recognition by 3A06 which
138 is distinct relative to previously reported quaternary epitope dependent DENV and ZIKV mAbs
139 C10 [22], SIgN-3C [23], ZIKV-195 [24], and ADI30056 [25] (**Figure S7**). Together, these observations reveal
140 structural features that distinguish the mode of interaction from previously characterized EDE-
141 specific antibodies, such as the EDE1-C10 antibody.

142 **Somatic hypermutations in the 3A06 light chain strongly influence antigen recognition**
143 **and neutralization**

144 We further examined how somatic hypermutations (SHM) in the heavy (VH) and light
145 (VL) chain variable regions contribute to neutralization and antigen recognition. To address this,
146 we generated antibodies in which the VH region, the VL region, or both were reverted to their
147 inferred germline sequences (iGL) as shown in (**Figure 4A**), allowing us to dissect the relative
148 contributions of each chain to antigen recognition and neutralization potency. The iGLs were
149 designed by reverting the VH or VL to their germline sequences while retaining the original
150 CDRH3 and CDRL3 sequences based on sequence alignments generated by IMGT sequence
151 analysis (**Figure S8**). Additionally, we evaluated the 3A06 antibody mutation probabilities using
152 ARMADiLLO, which is an online server for identifying probable and improbable mutations [26]. The
153 improbable mutations (Imp) are low-probability amino acid changes determined by
154 ARMADiLLO, which are amino acid substitutions in antibody variable regions that have a low

155 probability (2% or lower) of occurring during the natural somatic hypermutation process,
156 because they require multiple nucleotide changes [26]. This analysis resulted in the identification
157 of four improbable mutations in both the VH and VL genes ranging from 1-2% frequency in the
158 3A06 antibody (**Figure S6A-B**). Based on these analyses we generated additional combinations
159 of 3A06 VH and/or VL chain genes with only the improbable mutation reverted to germline gene
160 sequences (**Figure 4B**).

161 We found that antibodies based on the light chain variable region (iGL and Imp variants)
162 are important for recognizing antigens. In comparison to the heavy chain-based variants, the
163 light chain variants showed little or no binding to DENV2 and ZIKV E-protein dimers (**Figure 4C**
164 **and S9**). The VH reverted 3A06 IgG1 antibody showed reduced neutralizing activity against both
165 ZIKV and DENV2. However, the VL reverted and VH-VL reverted iGL 3A06 antibodies showed no
166 neutralizing activity against ZIKV or DENV2 (**Figure 4D**). Similarly, the VH-Imp reverted 3A06
167 IgG1 antibody showed reduced neutralization potential against both ZIKV and DENV2. In
168 comparison, the VL-Imp reverted antibody showed substantial reduction in neutralizing activity
169 against DENV2 compared to wild-type 3A06 IgG1 antibody (**Figure 4D**). The VH VL-Imp reverted
170 3A06 antibody showed reduction in neutralization against ZIKV. Against DENV2, the VH VL-Imp
171 reverted 3A06 antibody did not show any neutralization compared to the wild-type 3A06 IgG1
172 antibody (**Figure 4D**). Moreover, reversion of these key SHMs resulted in increased infection in
173 U937 cells at sub-neutralizing concentrations, suggesting that affinity maturation modulate the
174 balance between neutralization and enhancement in these assays (**Figure 4E and 4F**). These
175 results demonstrate that SHMs in the 3A06 light chain variable gene make a major contribution
176 to antigen recognition and neutralization potency against both DENV2 and ZIKV. Reversion of
177 specific low-probability or improbable mutations markedly reduced neutralization potency,
178 suggesting that affinity maturation of the light chain plays an important role in shaping the
179 functional activity of 3A06 antibody.

180 **3A06 is encoded by an uncommon combination of antibody variable genes**

181 We next investigated the genetic basis of the structural and functional properties
182 exhibited by 3A06. Sequence analysis of the variable regions revealed that 3A06 is encoded by a
183 combination of heavy and light chain immunoglobulin genes not commonly observed among
184 other flavivirus broadly neutralizing antibodies, including those targeting EDE1 (EDE1-C8, C10),
185 EDE2 (EDE2-B7, A11), or other quaternary epitopes (SIgN-3C) (**Table 1 and Figure S8**). The
186 heavy chain variable region is derived from IGHV4-61*01, IGHD4-17*01, and IGHJ5*01, while
187 the light chain derived from IGLV1-44*01, IGHJ3*01 gene. The 3A06 heavy chain exhibits
188 moderately high levels of somatic hypermutation (11.34%) compared to previously reported E-
189 dimer specific mAbs. The light chain is somewhat less mutated (6.32%). 3A06 has a CDR3 length
190 of 18 amino acids, and 11 amino acids in CDRL3 region, which are comparable to EDE1 specific
191 antibodies EDE1-C10 and EDE1-C8 [5]. The IGHV and IGLV gene combination seen in 3A06 may
192 help explain why it recognizes its target differently from previously reported antibodies that
193 bind quaternary epitopes. This also suggests that 3A06 arises from a gene pairing that is
194 relatively uncommon.

195 **3A06 expressed in IgG3 subclass broadens neutralization against dengue and zika viruses**

196 We next investigated whether antibody subclass influences the functional breadth of
197 3A06. While the IgG1 form effectively neutralizes DENV1-3 and ZIKV, it shows no detectable
198 neutralization of DENV4. To determine whether Fc architecture could modulate this activity, we
199 additionally generated IgG2, IgG3, and IgG4 variants and assessed their neutralization profiles
200 across all four dengue serotypes (**Figure 5A**). In contrast to 3A06 IgG1, the IgG3 version showed
201 higher binding to sE protein dimers of all four DENV serotypes and ZIKV (**Figure 5B and Figure**
202 **S10**) and potent neutralization activity against DENV4 (**Figure 5C**), which was resistant to
203 neutralization by 3A06 IgG1. Further, to assess the potential for 3A06 mediated ADE, we

204 performed DENV2 and ZIKV infection assays using Fcγ receptor expressing U937 cells pre-
205 incubated with varying concentrations of 3A06 in various Fc variants. The 3A06 IgG1 variant
206 mediated moderate enhancement of DENV2 and ZIKV infection at sub-neutralizing
207 concentrations (**Figure 5D**). In contrast, the IgG3 version induced higher levels of DENV2 and
208 ZIKV ADE. The IgG2 subclass antibody didn't mediate enhancement, consistent with its low
209 affinity for Fcγ receptors [27,28].

210 Based on these observations, we next engineered the L234A/L235A/P329G (LALA-PG)
211 Fc variant of the 3A06 antibody in both IgG1 and IgG3 subclasses. The LALA-PG Fc mutant is well-
212 known to abrogate Fcγ receptor binding in IgG1, and here we grafted the same mutations into
213 IgG3 to determine whether these could also abolish Fcγ receptor binding in the IgG3 Fc
214 backbone. We did not observe any change in neutralization activity between the LALA-PG IgG1
215 and IgG3 antibodies compared to their respective wild-type antibodies (**Figure 5C**). As expected,
216 IgG1 LALA-PG antibody completely eliminated ADE. Interestingly, the same mutations
217 incorporated into the IgG3 version were also effective in silencing ADE (**Figure 5D**). These
218 findings indicate that antibody IgG3 subclass conversion influences the quaternary epitope
219 accessibility, and functional neutralization breadth.

220 **3A06 IgG3 hinge architecture facilitates bivalent virion engagement**

221 In order to understand the unique capacity of 3A06 to bind and neutralize DENV4 when
222 presented on an IgG3 backbone, we performed cryo-EM of whole IgG3 in complex with chimeric
223 DENV2-BinJV and chimeric DENV4-BinJV and compared these to ZIKV-BinJV and DENV2-BinJV
224 complexed with 3A06 Fab. Whole IgG3 format mAbs were purified by protein G and complexed
225 with virions. Cryo-EM datasets were collected and complexes resolved by SPA. We determined
226 cryo-EM structures of IgG3-bDENV2 at 4.4 Å resolution and IgG3-bDENV4 at 4.17 Å resolution.
227 Comparing the resulting maps, the antibody density was the lowest for DENV2 complexed with

228 3A06 Fab, followed by DENV4 3A06 IgG3, DENV2 3A06 IgG3 and ZIKV 3A06 (**Figure 6A, Figure**
229 **S2 and Table S2**), consistent with the observed binding levels. Similar to ZIKV, no antibody
230 density was observed at the 5-fold proximal site, which results from a clash across the E rafts,
231 and this configuration also abrogates the intra-dimer LC contacts critical for 3A06 binding.
232 Although the occupancy was improved for the DENV2 bound to intact IgG3 compared with Fab
233 alone, no clear Fc or hinge density was observed, most likely due to the inherent flexibility of
234 these regions. Interestingly, extra density around the CH1 and CL domains was observed for
235 DENV2 complexed with 3A06 IgG3 when compared to ZIKV and Fab (**Figure 6B, green**). In order
236 to examine this in more detail, focused classification was carried out using symmetry expanded
237 particle sets, focusing on either side of the CH1 and CL domains (**Figure 6B dashed circles**). This
238 revealed two distinct classes, where the Fab densities at the 3-fold proximal site can adopt either
239 a conformation with the CH1 and CL domains bent over towards the adjacent 2-fold position
240 within the E raft (**Figure 6C, class 1**) or a conformation similar to the 3-fold site Fab (**Figure 6C,**
241 **class 2**). These two conformations alter the relative positions of the CH1 linker region and
242 therefore influence the potential for bivalent engagement of the full antibody molecule (**Figure**
243 **6D, Figure S11**). Notably, we observed Fab densities at the 2-fold position (intra-raft) in both
244 classifications, while the antibody density at the adjacent 3-fold position (inter-raft) was
245 stronger in the 2nd class, consistent with the ability of the IgG3 to bind across the E rafts when in
246 this more favorable CH1-CL conformation. This is different to what has been previously observed
247 for DENV mAb C10 when complexed with virions as a F(ab)2' [22], where only a single bivalent
248 binding mode was observed with C10 adopting a conformation similar to our observed Class 1,
249 but with no clear densities at the 2-fold sites. To examine this difference further, we investigated
250 the relative distances of the first disulfide position of the hinge for C10 and 3A06 in IgG1 and
251 IgG3 framework (**Figure S12**). We found that the hinge disulfide is least favorable for 3A06 in
252 the IgG1 format, followed by C10. In contrast, in the IgG3 format, 3A06 readily retains the hinge

253 disulfide while simultaneously engaging both 3-fold proximal epitopes within a raft. Based on
254 these findings, the inability of 3A06 IgG1 to neutralize DENV4 is likely due to structural
255 constraints that prevent effective multivalent binding to the virion. In contrast, the longer and
256 more flexible hinge region of IgG3 enables it to span and engage multiple sites across the virion
257 more effectively. This increased flexibility enhances binding strength or avidity and overall
258 functional activity, thereby permitting neutralization. Overall, these results indicate that the
259 extended hinge architecture of the IgG3 subclass facilitates bivalent engagement of the virion in
260 multiple configurations, leading to expanded neutralization breadth.

261 **DISCUSSION**

262 The comprehensive characterization of 3A06 as a quaternary E-protein conformation
263 specific human monoclonal antibody with potent DENV and ZIKV cross-neutralizing capacity
264 offers several conceptual advances. First, it advances the existing knowledge that heavy chain
265 dominated paratopes primarily determine antigen specificity in anti-flavivirus antibodies. In the
266 case of 3A06, we find that antigen binding, and neutralization potency are critically dependent
267 on the light chain, as confirmed by functional assays based on chimeric constructs encoding iGL
268 variants and improbable mutations reverted 3A06 antibody variants. Such light chain dependent
269 interactions compared to previously described antibodies in which light chain contributions are
270 more evenly distributed may open new avenues for epitope focused flavivirus vaccine design
271 and antibody optimization strategies.

272 Second, our results show that IgG subclass plays an important role in shaping both
273 neutralization breadth and antibody-dependent enhancement for 3A06. In the IgG1 format, 3A06
274 neutralizes DENV1-3 and ZIKV but does not neutralize DENV4, a serotype that is often less
275 sensitive to broadly neutralizing antibodies. When expressed as IgG3, however, 3A06 gains the
276 ability to neutralize all four DENV serotypes. This difference can be explained by structural
277 features of the IgG3 hinge, which increase flexibility and allow more effective engagement of
278 epitopes on the virion surface. Our cryo-EM analysis of intact 3A06 IgG3 in complex with DENV
279 particles supports this interpretation. The data show that movement of the CH1 and CL domains
280 at the 3-fold site allows the antibody to adopt more than one binding configuration, enabling
281 engagement of both intra-raft and inter-raft epitopes. This behavior differs from what has been
282 reported for the C10 antibody, where binding is limited to a single intra-raft configuration [22].
283 These observations suggest that the IgG3 format enhances the ability of 3A06 to interact with
284 the complex quaternary epitope present on DENV4. A central conclusion from this work is that

285 the lack of DENV4 neutralization by 3A06 IgG1 is not due to a failure to recognize the epitope.
286 Instead, it reflects an inability to meet the spatial requirements needed for effective binding.

287 The 3A06 epitope spans both 2-fold and 3-fold proximal regions, and neutralization
288 requires bivalent engagement across E protein rafts. This creates a geometry-dependent
289 requirement in which the antibody must bridge specific distances and orientations between
290 adjacent sites. For DENV4, these constraints appear to be more restrictive. The shorter and less
291 flexible hinge of IgG1 likely limits its ability to adopt conformations that support binding across
292 rafts, resulting in predominantly monovalent interactions that are not sufficient for
293 neutralization. In contrast, the longer hinge of IgG3 allows a wider range of Fab orientations,
294 including those that support cross-raft binding. This enables stable bivalent engagement and
295 increases overall binding strength, which allows neutralization to occur. Together, these findings
296 define a subclass-dependent mechanism in which neutralization is influenced not only by
297 epitope recognition but also by the physical properties of the antibody. More broadly, these
298 results show that DENV4 is not escaping recognition by 3A06, but rather limiting the antibody's
299 ability to engage both binding sites at the same time. The IgG3 format overcomes this constraint
300 by providing the flexibility needed for effective bivalent binding. In addition, we show that LALA-
301 PG mutations effectively abrogate ADE in U937 cells in the IgG3 format, consistent with their
302 established effects in IgG1 [28–30]. This result indicates that Fc effector functions can be selectively
303 minimized in IgG3 without disrupting its structural advantages for antigen engagement. Such
304 control may be particularly important in the context of flaviviruses, where FcγR interactions
305 contribute to ADE. Together, these findings support the feasibility of combining subclass-specific
306 properties with Fc engineering to optimize antibody function.

307 The rare germline gene usage of 3A06 further supports the idea that some of the most
308 effective broadly neutralizing antibodies arise from uncommon B cell lineages. The IGHV4-

309 61/IGLV1-44 combination observed here is not reported in known DENV/ZIKV antibodies
310 targeting the conformational epitopes present on the dimeric state of the E-protein. This
311 highlights the possibility that natural DENV infection resulted in induction of E-dimer specific
312 antibodies comprising different unbiased immunogenetic features. These findings highlight the
313 need for expanded profiling of underrepresented B cell clones and non-public clonotypes. The
314 quaternary epitope recognized by 3A06 is present only on intact virions and is not reproduced
315 by monomeric E protein, suggesting that vaccine antigens must preserve native E-protein
316 organization that is present on mature virions to elicit similar antibodies.

317 In summary, this study defines the structural and functional features of the human
318 monoclonal antibody 3A06, which recognizes a quaternary epitope spanning three E protein
319 protomers on the flavivirus surface. Structural analysis shows that 3A06 engages this interface
320 through coordinated contacts involving both heavy and light chains. Functional data further
321 demonstrate that mutations in the light chain make a substantial contribution to antigen
322 recognition and neutralization potency. We also show that antibody subclass can influence
323 antiviral activity. The IgG3 format, with its longer and more flexible hinge, supports bivalent
324 engagement of adjacent epitopes on the virion surface and expands neutralization breadth,
325 including activity against DENV4 that is not observed in the IgG1 form. These findings highlight
326 how both paratope composition and antibody architecture shape recognition of quaternary
327 epitopes on flavivirus particles. Therefore, our findings suggest that IgG3-based antibody
328 formats may offer potential advantages when targeting structurally complex or spatially
329 constrained epitopes on flaviviruses and other viruses, such as HIV, influenza virus, and SARS-
330 CoV-2, where epitope accessibility is shaped by virion architecture. While these implications
331 require further study, our findings support continued structural and functional evaluation of
332 IgG3 antibodies across different viral systems. Together, this work provides a framework for
333 understanding how antibody structure relates to function and may guide the design of vaccines

334 and therapeutic antibodies with improved breadth and potency against flaviviruses and related

335 pathogens.

336 **METHOD DETAILS**

337 **Cell lines**

338 Vero CCL-81 cells (ATCC), were maintained in Eagle's Minimum Essential Medium
339 (EMEM) (ATCC) medium supplemented with 10% fetal bovine serum (FBS) (HyClone) and
340 antibiotic-antimycotic (1X) (Gibco). U937 cells (ATCC) were maintained in RPMI-1640
341 supplemented with 10% FBS, 2mM L-Glutamine (Gibco), 1mM 4-(2-hydroxyethyl)-1-
342 piperazineethanesulfonic acid (HEPES) (Gibco), 1mM sodium pyruvate (Gibco), 1X Non-essential
343 Amino Acids (NEAA) (Gibco) and 1X penicillin/streptomycin (Gibco). All these cells were
344 cultured at 37°C with 5% CO_2. The expi293™ cells (Gibco) were maintained in expi293
345 expression medium (Gibco) and cultured at 37°C, 125 rpm shaking and 8% CO_2.

346 **DENV and ZIKV amplification and lysate preparation**

347 DENV1 strain WestPac74, DENV2 strain 16681, DENV3 strain 3001, DENV4 strain Sri
348 Lanka 92 and ZIKV strain PRVABC59 was obtained from the Centers for Disease Control and
349 Prevention (CDC) and was passaged by infecting Vero CCL-81 cells at a multiplicity of infection
350 (MOI) of 0.1 in EMEM (ATCC). After a 1 h infection at 37°C, the virus inoculum was removed and
351 EMEM supplemented with 10% FBS and 1% antibiotic-antimycotic (1X) (Gibco) was added to
352 the cells. Upon observation of severe cytopathic effect (CPE) 4 to 6 days (DENVs) and 48 hr for
353 ZIKV, supernatants were collected and spun down at 4000 × g for 10 min at 4°C. Supernatant
354 containing virus was supplemented with an additional 10% (vol/vol) FBS before freezing at –80
355 °C. Viruses were titred by focus forming assay on Vero CCL-81 cells before use.

356 The viral lysates were prepared as described previously [7]. Briefly, to prepare all four
357 DENV1-4 serotypes and ZIKV lysates, the remaining Vero CCL81 adherent cells and cell pellet
358 from the virus-containing supernatant were washed twice with Dulbecco's Phosphate Buffer

359 Saline (DPBS) and then resuspended in the cell lysis buffer (10 mM Tris, 150 mM NaCl, 1%
360 sodium deoxycholate, 1% Triton X-100, pH 7.4) supplemented with protease inhibitor (Thermo
361 Fisher Scientific) and phosphatase inhibitor (Biovision). Mock lysate was prepared in a similar
362 fashion with uninfected cells. Bradford assay was performed to quantitate total protein yield.

363 **Dimeric DENV and ZIKV Env antigen expression and purification**

364 All four serotypes DENV1-4, and ZIKV dimeric Env constructs were designed by
365 incorporating dimer stabilizing disulfide bonds based on previous designs [3] with a c-terminal
366 strep-tag II sequence were synthesized and cloned in pTwist Beta Glo Neo expression vector from
367 Twist Biosciences. Transfections were performed as per the manufacturer's protocol in expi293
368 cells (Thermo Fisher). Briefly, expi293 cells were seeded at a density of $2x10^6$ cells/ml in Expi293
369 expression medium and incubated at 37°C and 125 rpm with 8% CO_2 overnight. The next day,
370 $2.5x10^6$ cells/ml were transfected using ExpiFectamine™ 293 transfection reagent
371 (ThermoFisher). Next morning, enhancers 1 and 2 were added along with 0.5% of antibiotic-
372 antimycotic solution (Gibco). The cells continued to grow for 5 days at 37°C, 125 rpm, 8% CO_2
373 incubator. The cells were removed by centrifugation at 6,000g for 20 minutes at room
374 temperature and dimeric env protein-containing supernatant was collected. The supernatant
375 was filtered through 0.45 um filter assembly (VWR) and loaded onto pre-washed Strep-
376 Tactin®XT 4Flow® resin (IBA Lifesciences) for affinity purification. Resin washed with 1x wash
377 Buffer (buffer W) containing 25mM Tris, 150mM NaCl and 1mM EDTA with pH 8.0 followed by
378 Env protein elution in elution buffer 1x BXT buffer (IBA). Eluted protein dialyzed against DPBS
379 and concentrated. The concentrated protein ran onto a Superdex200 Increase 10/300 column
380 and protein eluted as dimeric Env collected.

381

382

383 **Monoclonal Antibody Expression and Purification**

384 Human mAbs used in study were generated as previously described [7,12]. First, 3A06, IgG
385 subclasses variants (IgG1, IgG2, IgG3 and IgG4) and IgG1 Fc variants, L234A/L235A/P329G
386 (LALA-PG) [29,30], were generated by replacing the constant region of the wild-type IgG1 heavy
387 chain expression vector with synthesized constructs (Twist Bioscience). The variable heavy and
388 light chain sequences of control antibodies EDE1-C10 [16], and EDE2-A11 [5] were synthesized
389 (Twist Bioscience) and cloned into human IgG1 expression vectors based on PDB IDs 7A3N and
390 5N0A respectively. Next, the variable heavy and light chain sequences encoding expression
391 plasmids were transiently expressed in expi293F cells for 5 days and secreted antibodies were
392 purified from supernatants using protein A coupled sepharose beads (Pierce) as per
393 manufacturer's instructions.

394 **ELISA assays**

395 The binding potential of mAbs to ZIKV and DENV E protein antigens (Monomer, EDIII
396 domain) and viral lysates was determined by ELISA. Briefly, the recombinant DENV1-4, ZIKV
397 antigens and viral lysates were coated in separate Nunc Maxisorp ELISA plates (Thermo
398 Scientific) at a concentration of 1 μg/ml in DPBS overnight at 4°C. Next morning, the plates were
399 washed thrice with DPBS containing 0.05% Tween-20 (DPBST) and blocked with DPBST
400 containing 1% BSA (ELISA buffer) for 1.5 hr at room temperature. Then, mAbs with serial 3-fold
401 dilution in ELISA buffer, starting at 10 μg/ml concentration were added to the plates and
402 incubated at room temperature for 1.5 h. The plates were washed thrice with DPBST, and the IgG
403 signals were detected by incubating with peroxidase-conjugated anti-human IgG (Jackson
404 ImmunoResearch) for 1 h. The plates were washed thrice with DPBST and developed using an o-
405 phenylenediamine substrate (Sigma) in 0.05M phosphate-citrate buffer (Sigma Aldrich)

406 containing 0.012% hydrogen peroxide. The absorbance values were measured at O.D. 490 nm.
407 The absorbance values were plotted against the concentration of antibodies.

408 DENV and ZIKV E-protein dimer-based ELISA assays were performed using
409 StrepTactinXT coated plates. StrepTactinXT coated microplates (IBA lifesciences) do not require
410 any functionalization or blocking steps prior to protein immobilization. Briefly, 100 µL of Strep-
411 Tagged purified E-protein dimers in ELISA buffer at 1 µg/mL concentration were dispensed in
412 the corresponding wells for protein immobilization by a 2 h incubation at room temperature.
413 Following a triple wash with DPBST to remove unbound proteins, three-fold serial dilutions of
414 test mAbs and control mAbs (EDE1-C10, EDE2-A11, Z004 and 4G2) starting at 10 µg/ml
415 concentration in ELISA buffer were added and incubated for 1.5 h at room temperature. After 3
416 washes with DPBST, peroxidase-conjugated anti-human IgG (Jackson Immunoresearch) diluted
417 1:3000 in ELISA buffer was added and incubated for 1 h, followed by three washes with DPBST.
418 Plates were developed with o-phenylenediamine substrate (Sigma-Aldrich) in 0.05 M
419 phosphate-citrate buffer (Sigma-Aldrich) pH 5.0, containing 0.012% hydrogen peroxide
420 (Thermo Fisher Scientific). Absorbance was measured at 490 nm to obtain the binding data.

421 **Octet BLI analysis**

422 Octet biolayer interferometry (BLI) was performed using an Octet Red96 instrument
423 (ForteBio, Inc.). Briefly, mAbs were captured on ProA biosensors at 5 µg/ml concentration in BLI
424 running buffer (0.1% BSA, 0.001% Tween20 in 1x DPBS). Binding kinetics were tested with serial
425 2-fold serially diluted DENV1-4 and ZIKV E-protein dimers (100 nM to 6.25 nM). The baseline
426 was obtained by measurements taken for 120 s in BLI running buffer. The biosensors were
427 dipped to obtain association phase for 300 s in wells containing serial dilutions of E-protein
428 dimers. Then, the sensors were immersed in BLI running buffer for as long as 600 s to measure
429 the dissociation phase. Sensors were regenerated in glycine pH 2.0 buffer and immediately

430 neutralized by dipping in Tris pH 9.0 buffer. The mean K_{on}, K_{off} and apparent KD values of the
431 mAbs binding affinities for E-protein dimers were calculated from all the binding curves based
432 on their global fit to a 1:1 Langmuir binding model using Octet software version 12.0.

433 **Preparation of 4G2 Antibody**

434 Pan-flavivirus anti-envelope mAb 4G2 was isolated from the supernatant of mouse
435 hybridoma (D1-4G2-4–15; ATCC) grown in hybridoma medium (Thermofisher Scientific), and
436 purified using protein G beads (Pierce) according to the manufacturer's recommendations. The
437 antibodies were stored in 1x PBS for in-vitro cell culture assays and with 0.05% sodium azide at
438 4°C for the binding assays.

439 **Live virus-based focus reduction neutralization test (FRNT) assays**

440 The neutralization potential of mAbs and serum samples was determined by FRNT as
441 described previously [7] with a few modifications. Two-fold serially diluted mAbs starting at
442 20 µg/ml concentration were incubated with a previously titrated amount of virus (~100 focus
443 forming units) of ZIKV or DENV1-4 for 1 h at 37 °C. Vero CCL81 cell monolayers in 96-well plates
444 were subsequently infected with the mixture for 1 h at 37 °C. An overlay containing 1% (wt/vol)
445 methylcellulose (Sigma) was added to the cells. After 48 h (ZIKV) and 72 h (DENV) incubation at
446 37 °C, the cells were washed and fixed with a 1:1 mixture of acetone and methanol at room
447 temperature. Foci were stained using 4G2 at 0.5 µg/ml concentration for 2 h at room temperature
448 followed by HRP-linked anti-mouse IgG (Cell Signaling) for 1 h and developed using TrueBlue
449 Peroxidase substrate (KPL) for 2 h at room temperature. At each step, plates were washed thrice
450 with 1x DPBS and Foci were imaged using a CTL-Immunospot S6 Micro Analyzer.

451

452

453 **Antibody Dependent Enhancement (ADE) assay**

454 ADE assay was performed as described previously [7]. Briefly, serially diluted mAbs were
455 incubated with ZIKV with an MOI of 0.5 for 1 h at 37 °C. The immune complexes were added in a
456 96-well plate containing $2x10^4$ U937 cells (ATCC) per well in RPMI-1640 with 10% (vol/vol) FBS.
457 The Cells were infected for 24 h at 37 °C. The cells were then washed and fixed/permeabilized
458 using BD intracellular staining reagents Fix/Perm Solution (BD biosciences) and Perm/Wash
459 Buffer (BD biosciences) according to the manufacturer's protocol. Cells were stained with in-
460 house prepared 4G2 antibody conjugated to Alexa fluor 594 for 1h for 25 min. The percentage of
461 infected ($4G2^+$) cells was determined using flow cytometry using the Cytek Aurora flow
462 cytometer followed by analysis using FlowJo software v10.

463 **Virus and antibody purification for Cryo-EM**

464 Chimeric viruses containing the non-structural genes of Binjari virus (BinJV) and prME
465 genes of ZIKV (Natal, Genbank: NC_035889)), DENV-2 (ET300, Genbank: EF440433), and DENV-
466 4 (ET288, Genbank: EF440435) were generated using circular polymerase extension reaction as
467 previously described [19,20,31]. To ensure mature virion preparations the prM furin cleavage site of
468 DENV-2 and DENV-4 prME was modified to an Influenza H5 HA furin cleavage site (RERRRKKRS).
469 Virus recovered from transfected C6/36 cells were passaged to P1 and propagated in C6/36 cells
470 (MOI: 0.1). Clarified viral supernatant was then purified as previously described with PEG
471 precipitation, followed by a 20% sucrose cushion, and 25-40% potassium tartrate gradient [21,32].
472 Gradient fractions containing virus were then harvested and used for Cryo-EM imaging. Fab
473 fragments of 3A06 were generated by cloning the HV region of 3A06 into a mammalian
474 expression vector containing a C-terminal C-Tag (EPEA) [33,34]. Plasmids encoding the HV Fab and
475 LC were then transfected into ExpiCHO cells, incubated for 7 days at 37 °C shaking, with the

476 clarified supernatant then purified using an CaptureSelect™ C-tagXL Pre-packed Column on an
477 AKTA-Pure FPLC.

478 **Cryo-electron microscopy**

479 Chimeric flavivirus were complexed with excess 3A06 Fab fragments or IgG3 for 1 hour at
480 4 °C before being applied to glow discharged R3.5/1 holey carbon grids (Quantifoil). Grids were
481 then vitrified using an EM GP2 (Leica Microsystems) set at 4 °C and 95% relative humidity, grids
482 were pre-blotted for 10 secs, followed by blotting for 3 secs and immediately plunge-frozen in
483 liquid ethane. Grids were transferred under liquid nitrogen either to a CRYO ARM™ 300 (JEOL
484 JEM-Z300FSC) transmission electron microscope operated at 300 kV, equipped with a K3 direct
485 electron detector (Gatan) and an omega in-column energy filter operated at 20 eV (JEOL), or to a
486 CRYOARM™ 200 TEM operated at 200 kV, equipped with a K2 Summit direct electron detector
487 (Gatan) and an omega in-column energy filter operated as above. Movies on both microscopes
488 were recorded using SerialEM at 60,000 x magnification [35].

489 **Cryo-EM processing, single particle analysis, and model building**

490 Cryo-EM datasets were motion corrected, and the contrast transfer function (CTF)
491 parameters were estimated using *cis*TEM [36]. Virus-Ab particles were automatically picked,
492 extracted, and classified over multiple rounds of 2D classification. The initial 3D reconstructions
493 on *cis*TEM were caried out ab initio, followed by 3D refinement using the low-resolution ab into
494 model as a reference. High-resolution asymmetric focused reconstructions were carried out by
495 symmetry expansion using *cis*TEM as previously described [21,37]. Each image was subtracted 60
496 times using each of the 60 icosahedral ASUs generating a dataset of isolated asymmetric units
497 which were automatically centred. The dataset of ASUs was then further refined using *cis*TEM
498 without symmetry applied. The initial atomic model of bZIKV complexed with 3A06 Fab was
499 generated using an existing cryoEM structure of ZIKV virus (PDB: 6CO8) as a template with an

500 AlphFold3 generated model of 3A06 Fab. All modelling was performed using iterative cycles of
501 ISOLDE (v. 1.2.1), COOT (v.0.8.9.2), and PHENIX (v.1.19.2) [38–40]. The geometry and quality of the
502 model were evaluated through a combination of PHENIX and the wwPDB Validation system. For
503 focussed classification of bDENV-2 complexed with 3A06 IgG3, independent focussed
504 classification of the 3-fold proximal Fab fragment was performed by masking the density either
505 side of the 3-fold fab on the ASU followed by 3D classification using Relion 5.0.1. Particle stacks
506 of Relion classes were then reimported into cisTEM and manual 3D refinement was performed
507 to generate final focus classified ASU maps.

508 **Immunogenetic analyses of antibody genes and envelope protein sequence alignment**

509 The immunogenetic analysis of both heavy chain and light chain germline assignment,
510 framework region annotation, determination of somatic hypermutation (SHM) levels
511 (nucleotides) and CDR loop lengths (amino acids) was performed with the aid of IMGT/HighV-
512 QUEST (www.imgt.org/HighV-QUEST) [41,42]. The envelope protein sequence alignments were
513 done using the MAFFT version 7, a multiple alignment program for amino acid or nucleotide
514 sequences (https://mafft.cbrc.jp/alignment/server/index.html) [43,44].

515 **Statistical analysis**

516 Graphpad Prism version 9.0 was used for all statistical analyses.

517 **DATA AND MATERIALS AVAILABILITY**

518 Atomic coordinates and Cryo-EM maps for reported structures are deposited into the
519 Protein Data Bank (PDB) and the Electron Microscopy Data Bank (EMDB) with accession codes
520 PDB: 24ZZ and EMDB: 69949 for chimeric virus between Binjari virus and zika virus in complex
521 with 3A06 Fab; EMDB: 69863 for chimeric virus between Binjari virus and dengue virus
522 serotype-2 (ET300) in complex with 3A06 Fab; EMDB: 69785 for chimeric virus between Binjari

523 virus and dengue virus serotype-2 (ET300) in complex with 33.3A06 immunoglobulin G3; EMDB:
524 69800 for chimeric virus between Binjari virus and dengue virus serotype-4 in complex with
525 33.3A06 immunoglobulin G3. This paper does not report original code. All data needed to
526 evaluate the conclusions in the paper are present in the paper and/or the supplemental
527 information. Any material request or additional information required to reanalyze the data
528 reported in this paper is available from the corresponding author upon request.

529 **ACKNOWLEDGEMENTS**

530 We thank and acknowledge the facilities, and the scientific and technical assistance of the
531 Australian Microscopy & Microanalysis Research Facility at the Centre for Microscopy and
532 Microanalysis, The University of Queensland.

533 **FUNDING**

534 This work was funded in part by NIH/National Institute of Allergy and Infectious Diseases
535 (NIAID) Grants R01AI149486 (to J.W. and M.S.S.), R56AI110516 (to M.S.S.) and DBT/Wellcome
536 Trust India Alliance Early Career Fellowship grant IA/E/18/1/504307 (to S.K.).

537 **AUTHOR CONTRIBUTIONS**

538 Conceptualization, S.K., D.W., and J.W.; methodology, S.K., N.M., M.S.S., D.W., J.W.;
539 investigation, S.K., C.A.P.S., L.X., K.M., J.V.V., S.S., R.H.W., S.L.G., N.M.; visualization, N.M., M.S.S., D.W.,
540 J.W.; funding acquisition, S.K., M.S.S., D.W., J.W.; project administration, S.K., L.X., R.H.W.;
541 supervision, M.S.S., D.W., J.W.; writing – original draft, S.K., C.A.P.S., M.S.S., D.W. and J.W.; writing –
542 review & editing, all authors.

543 **DECLARATION OF INTERESTS**

544 All other authors declare no competing interests.

545 **FIGURES & FIGURE LEGENDS**

546 **Figure 1: 3A06 antibody selectively recognizes quaternary E-protein dimers and mediates**
547 **broad and potent neutralization. (A)** ELISA binding of 3A06 to recombinant E-protein dimers,
548 monomers, EDIII, and viral lysates. The dotted line represents the limit of detection. Here, EDE1-
549 C10 and EDE2-A11 antibodies were used as positive controls for E-dimers, FLE-specific antibody
550 4G2 was used here as control for E-monomers and viral lysates, and Z004 a ZIKV-EDIII specific
551 antibody was used as control for EDIII domain for ZIKV. **(B)** Live-virus based focus reduction
552 neutralization test (FRNT) assays data. **(C)** Biolayer interferometry (BLI) analysis reveals high-
553 affinity binding to E dimers, with heterogeneous kinetics.

554 **Figure 2: Cryo-EM structural analysis of 3A06 Fab in complex with ZIKV-BinJV. (A)** 4.6 Å
555 cryo-EM reconstruction of bZIKV complexed with 3A06 Fab colored by E domains (EDI: Red,
556 EDII: Yellow, EDIII: Blue) and Fab heavy variable (Magenta) and light variable (Pink) domains.
557 The asymmetric unit of bZIKV is labelled with the ellipses, triangles and pentagon representing
558 the 2-, 3- and 5-fold icosahedral axes. (**B)** 3.1 Å symmetry expanded reconstruction of a pair of
559 bZIKV E-M heterodimers complexed with 3A06 Fab. Density has been zoned to atomic model in
560 panel C to display key contact sites for two fab fragments. **(C)** Top and side view of atomic model
561 of bZIKV complexed with 3A06 Fab with insets highlighting key hydrogen bonds for 3A06 LV
562 (pink) and 3A06 HV (magenta).

563 **Figure 3: Binding footprint and conservation of the 3A06 Epitope. (A)** Top view surface
564 representation of 3A06 footprint on a pair of ZIKV E dimers with heavy chain variable region
565 (HV) (magenta) and light chain variable region (LV) (pink). Each E monomer is labelled by chain
566 (A, C, E, G) and with 5- and 3- fold symmetry axis. **(B)** The same model from **(A)** colored by
567 sequence conservation of residues across DENV serotypes and ZIKV E. Coloring generated using
568 Chimera X (v1.8). Footprint of 3A06 Fab shown in black outline. **(C)** Buried surface area plot

569 showing which 3A06 residues are interacting with ZIKV E colored by E protomer with hydrogen
570 (H) bonds labelled. Germline V-genes of both VH and VL are shown with the CDRs indicated.

571 **Figure 4: Neutralizing activity of 3A06 is primarily contributed by its light chain. (A)**
572 Pictorial presentation of 3A06 WT and its somatic hypermutation reverted iGL variants, variable
573 heavy chain gene reverted VH-Rev, variable light chain gene reverted VL-Rev and both variable
574 heavy and light chain genes reverted VH VL-Rev antibodies. **(B)** Pictorial of 3A06 WT and its
575 improbable mutations reverted Imp variants, variable heavy chain gene reverted VH-Imp,
576 variable light chain gene reverted VL-Imp and both variable heavy and light chain genes reverted
577 VH VL-Imp antibodies. **(C)** ELISA binding of 3A06 iGL and Imp antibodies. The dotted line
578 represents the limit of detection. **(D)** 3A06 iGL and Imp antibodies neutralization analysis by live-
579 virus based FRNT assay. **(E)** In-vitro ADE analysis of 3A06 variants against DENV2 and ZIKV using
580 U937 cells.

581 **Figure 5: 3A06 IgG3 antibody subclass version potently neutralizes DENV4. (A)** Pictorial
582 presentation of 3A06 IgG1, IgG2, IgG3 and IgG4 subclass antibodies. **(B)** ELISA binding of 3A06
583 IgG subclasses. The dotted line represents the limit of detection. **(C)** 3A06 neutralization analysis
584 by live-virus based FRNT assay. **(D)** In-vitro ADE analysis of 3A06 IgG subclasses against DENV2
585 and ZIKV using U937 cells.

586 **Figure 6: Cryo-EM structural analysis of 3A06 IgG3 complexed with DENV2 and DENV4. (A)**
587 Whole virion maps of bZIKV complexed with 3A06 Fab, bDENV2 complexed with intact 3A06
588 IgG3, bDENV-4 with intact 3A06 IgG3 and bDENV-2 complexed with 3A06 Fab. Virions colored in
589 greys representing the 3 E proteins in the asymmetric unit, with the 3A06 HC in magenta and LC
590 in pink. 2 different contour levels (mean+3σ top, mean+ σ below) are shown for each
591 reconstruction to highlight the occupancy differences of 3A06 for each complex**. (B)** Close up
592 view of the 3A06 densities shown for bZIKV:Fab (left) and bDENV2:IgG3 (right). Additional

593 densities observed only in the DENV2 IgG3 bound map are colored yellow for the position of the
594 N67 DENV glycan and green for an extra density adjacent to the 3-fold Fab constant domain. **(C)**
595 Focused classification of the extra densities revealed two conformations for the-fold Fab on IgG3
596 bound DENV2, consistent with two alternate bivalent interactions provided by the IgG3 Fc linker
597 reach. **(D)** Spatial arrangement of the Fab densities on the two conformations. Distances between
598 the Glu216 (Eu numbering) residues in the HC CH1 are shown for all potential bivalent
599 interactions that could be mediated by a single mAb.

600 **REFERENCES**

601 1. Bhatt, S., Gething, P.W., Brady, O.J., Messina, J.P., Farlow, A.W., Moyes, C.L., Drake, J.M.,
602 Brownstein, J.S., Hoen, A.G., Sankoh, O., et al. (2013). The global distribution and burden of
603 dengue. Nature *496*, 504–507. https://doi.org/10.1038/nature12060.

604 2. Aggarwal, C., Ahmed, H., Sharma, P., Reddy, E.S., Nayak, K., Singla, M., Maheshwari, D., Chawla,
605 Y.M., Panda, H., Rai, R.C., et al. (2024). Severe disease during both primary and secondary
606 dengue virus infections in pediatric populations. Nat Med *30*, 670–674.
607 https://doi.org/10.1038/s41591-024-02798-x.

608 3. Rouvinski, A., Dejnirattisai, W., Guardado-Calvo, P., Vaney, M.-C., Sharma, A., Duquerroy, S.,
609 Supasa, P., Wongwiwat, W., Haouz, A., Barba-Spaeth, G., et al. (2017). Covalently linked dengue
610 virus envelope glycoprotein dimers reduce exposure of the immunodominant fusion loop
611 epitope. Nat Commun *8*, 15411. https://doi.org/10.1038/ncomms15411.

612 4. Slon-Campos, J.L., Dejnirattisai, W., Jagger, B.W., López-Camacho, C., Wongwiwat, W., Durnell,
613 L.A., Winkler, E.S., Chen, R.E., Reyes-Sandoval, A., Rey, F.A., et al. (2019). A protective Zika virus
614 E-dimer-based subunit vaccine engineered to abrogate antibody-dependent enhancement of
615 dengue infection. Nat Immunol *20*, 1291–1298. https://doi.org/10.1038/s41590-019-0477-
616 z.

617 5. Dejnirattisai, W., Wongwiwat, W., Supasa, S., Zhang, X., Dai, X., Rouvinski, A., Jumnainsong, A.,
618 Edwards, C., Quyen, N.T.H., Duangchinda, T., et al. (2015). A new class of highly potent, broadly
619 neutralizing antibodies isolated from viremic patients infected with dengue virus. Nat
620 Immunol *16*, 170–177. https://doi.org/10.1038/ni.3058.

621 6. Barba-Spaeth, G., Dejnirattisai, W., Rouvinski, A., Vaney, M.-C., Medits, I., Sharma, A., Simon-
622 Lorière, E., Sakuntabhai, A., Cao-Lormeau, V.-M., Haouz, A., et al. (2016). Structural basis of

623 potent Zika-dengue virus antibody cross-neutralization. Nature *536*, 48–53.
624 https://doi.org/10.1038/nature18938.

625 7. Priyamvada, L., Quicke, K.M., Hudson, W.H., Onlamoon, N., Sewatanon, J., Edupuganti, S.,
626 Pattanapanyasat, K., Chokephaibulkit, K., Mulligan, M.J., Wilson, P.C., et al. (2016). Human
627 antibody responses after dengue virus infection are highly cross-reactive to Zika virus.
628 Proceedings of the National Academy of Sciences *113*, 7852–7857.
629 https://doi.org/10.1073/pnas.1607931113.

630 8. Dai, L., Xu, K., Li, J., Huang, Q., Song, J., Han, Y., Zheng, T., Gao, P., Lu, X., Yang, H., et al. (2021).
631 Protective Zika vaccines engineered to eliminate enhancement of dengue infection via
632 immunodominance switch. Nat Immunol *22*, 958–968. https://doi.org/10.1038/s41590-
633 021-00966-6.

634 9. Kudlacek, S.T., Metz, S., Thiono, D., Payne, A.M., Phan, T.T.N., Tian, S., Forsberg, L.J., Maguire, J.,
635 Seim, I., Zhang, S., et al. (2021). Designed, highly expressing, thermostable dengue virus 2
636 envelope protein dimers elicit quaternary epitope antibodies. Sci Adv *7*, eabg4084.
637 https://doi.org/10.1126/sciadv.abg4084.

638 10. Kuhn, R.J., Zhang, W., Rossmann, M.G., Pletnev, S.V., Corver, J., Lenches, E., Jones, C.T.,
639 Mukhopadhyay, S., Chipman, P.R., Strauss, E.G., et al. (2002). Structure of dengue virus:
640 implications for flavivirus organization, maturation, and fusion. Cell *108*, 717–725.
641 https://doi.org/10.1016/s0092-8674(02)00660-8.

642 11. Zhang, X., Sheng, J., Plevka, P., Kuhn, R.J., Diamond, M.S., and Rossmann, M.G. (2013). Dengue
643 structure differs at the temperatures of its human and mosquito hosts. Proceedings of the
644 National Academy of Sciences *110*, 6795–6799. https://doi.org/10.1073/pnas.1304300110.

645 12. Priyamvada, L., Cho, A., Onlamoon, N., Zheng, N.-Y., Huang, M., Kovalenkov, Y., Chokephaibulkit,
646 K., Angkasekwinai, N., Pattanapanyasat, K., Ahmed, R., et al. (2016). B Cell Responses during
647 Secondary Dengue Virus Infection Are Dominated by Highly Cross-Reactive, Memory-Derived
648 Plasmablasts. J Virol *90*, 5574–5585. https://doi.org/10.1128/JVI.03203-15.

649 13. Rouvinski, A., Guardado-Calvo, P., Barba-Spaeth, G., Duquerroy, S., Vaney, M.-C., Kikuti, C.M.,
650 Navarro Sanchez, M.E., Dejnirattisai, W., Wongwiwat, W., Haouz, A., et al. (2015). Recognition
651 determinants of broadly neutralizing human antibodies against dengue viruses. Nature *520*,
652 109–113. https://doi.org/10.1038/nature14130.

653 14. Abbink, P., Larocca, R.A., Dejnirattisai, W., Peterson, R., Nkolola, J.P., Borducchi, E.N., Supasa, P.,
654 Mongkolsapaya, J., Screaton, G.R., and Barouch, D.H. (2018). Therapeutic and protective
655 efficacy of a dengue antibody against Zika infection in rhesus monkeys. Nat Med *24*, 721–723.
656 https://doi.org/10.1038/s41591-018-0056-0.

657 15. Fernandez, E., Dejnirattisai, W., Cao, B., Scheaffer, S.M., Supasa, P., Wongwiwat, W., Esakky, P.,
658 Drury, A., Mongkolsapaya, J., Moley, K.H., et al. (2017). Human antibodies to the dengue virus
659 E-dimer epitope have therapeutic activity against Zika virus infection. Nat Immunol *18*, 1261–
660 1269. https://doi.org/10.1038/ni.3849.

661 16. Sharma, A., Zhang, X., Dejnirattisai, W., Dai, X., Gong, D., Wongwiwat, W., Duquerroy, S.,
662 Rouvinski, A., Vaney, M.-C., Guardado-Calvo, P., et al. (2021). The epitope arrangement on
663 flavivirus particles contributes to Mab C10's extraordinary neutralization breadth across Zika
664 and dengue viruses. Cell *184*, 6052-6066.e18. https://doi.org/10.1016/j.cell.2021.11.010.

665 17. Dussupt, V., Modjarrad, K., and Krebs, S.J. (2021). Landscape of Monoclonal Antibodies
666 Targeting Zika and Dengue: Therapeutic Solutions and Critical Insights for Vaccine
667 Development. Front. Immunol. *11*. https://doi.org/10.3389/fimmu.2020.621043.

668 18. Dussupt, V., Sankhala, R.S., Gromowski, G.D., Donofrio, G., De La Barrera, R.A., Larocca, R.A.,
669 Zaky, W., Mendez-Rivera, L., Choe, M., Davidson, E., et al. (2020). Potent Zika and dengue cross-
670 neutralizing antibodies induced by Zika vaccination in a dengue-experienced donor. Nat Med
671 *26*, 228–235. https://doi.org/10.1038/s41591-019-0746-2.

672 19. Hardy, J.M., Newton, N.D., Modhiran, N., Scott, C.A.P., Venugopal, H., Vet, L.J., Young, P.R., Hall,
673 R.A., Hobson-Peters, J., Coulibaly, F., et al. (2021). A unified route for flavivirus structures
674 uncovers essential pocket factors conserved across pathogenic viruses. Nat Commun *12*,
675 3266. https://doi.org/10.1038/s41467-021-22773-1.

676 20. Hobson-Peters, J., Harrison, J.J., Watterson, D., Hazlewood, J.E., Vet, L.J., Newton, N.D.,
677 Warrilow, D., Colmant, A.M.G., Taylor, C., Huang, B., et al. (2019). A recombinant platform for
678 flavivirus vaccines and diagnostics using chimeras of a new insect-specific virus. Science
679 Translational Medicine *11*, eaax7888. https://doi.org/10.1126/scitranslmed.aax7888.

680 21. Bibby, S., Jung, J., Low, Y.S., Amarilla, A.A., Newton, N.D., Scott, C.A.P., Balk, J., Ting, Y.T., Freney,
681 M.E., Liang, B., et al. (2025). A single residue in the yellow fever virus envelope protein
682 modulates virion architecture and antigenicity. Nat Commun *16*, 8449.
683 https://doi.org/10.1038/s41467-025-63038-5.

684 22. Lim, X.-X., Shu, B., Zhang, S., Tan, A.W.K., Ng, T.-S., Lim, X.-N., Chew, V.S.-Y., Shi, J., Screaton, G.R.,
685 Lok, S.-M., et al. (2021). Human antibody C10 neutralizes by diminishing Zika but enhancing
686 dengue virus dynamics. Cell *184*, 6067-6080.e13.
687 https://doi.org/10.1016/j.cell.2021.11.009.

688 23. Zhang, S., Loy, T., Ng, T.-S., Lim, X.-N., Chew, S.-Y.V., Tan, T.Y., Xu, M., Kostyuchenko, V.A., Tukijan,
689 F., Shi, J., et al. (2020). A Human Antibody Neutralizes Different Flaviviruses by Using Different
690 Mechanisms. Cell Reports *31*, 107584. https://doi.org/10.1016/j.celrep.2020.107584.

691 24. Long, F., Doyle, M., Fernandez, E., Miller, A.S., Klose, T., Sevvana, M., Bryan, A., Davidson, E.,
692 Doranz, B.J., Kuhn, R.J., et al. (2019). Structural basis of a potent human monoclonal antibody
693 against Zika virus targeting a quaternary epitope. Proceedings of the National Academy of
694 Sciences *116*, 1591–1596. https://doi.org/10.1073/pnas.1815432116.

695 25. Sevvana, M., Rogers, T.F., Miller, A.S., Long, F., Klose, T., Beutler, N., Lai, Y.-C., Parren, M., Walker,
696 L.M., Buda, G., et al. (2020). Structural Basis of Zika Virus Specific Neutralization in
697 Subsequent Flavivirus Infections. Viruses *12*, 1346. https://doi.org/10.3390/v12121346.

698 26. Martin Beem, J.S., Venkatayogi, S., Haynes, B.F., and Wiehe, K. (2023). ARMADiLLO: a web
699 server for analyzing antibody mutation probabilities. Nucleic Acids Research *51*, W51–W56.
700 https://doi.org/10.1093/nar/gkad398.

701 27. Boesch, A.W., Miles, A.R., Chan, Y.N., Osei-Owusu, N.Y., and Ackerman, M.E. (2017). IgG Fc
702 variant cross-reactivity between human and rhesus macaque FcγRs. mAbs *9*, 455–465.
703 https://doi.org/10.1080/19420862.2016.1274845.

704 28. Xu, L., Kumar, S., Moore, K.M., Vander Velden, J.W., Mbadugha, F.A., Wang, M., Hailstorks, T.,
705 Sundberg, E.J., Sastre, D.E., Suthar, M.S., et al. (2025). FcγRI is the key determinant of antibody-
706 mediated Zika virus infection of human placental macrophages. bioRxiv, 2025.10.23.684201.
707 https://doi.org/10.1101/2025.10.23.684201.

708 29. Saunders, K.O. (2019). Conceptual Approaches to Modulating Antibody Effector Functions
709 and Circulation Half-Life. Front Immunol *10*, 1296.
710 https://doi.org/10.3389/fimmu.2019.01296.

711 30. Schlothauer, T., Herter, S., Koller, C.F., Grau-Richards, S., Steinhart, V., Spick, C., Kubbies, M.,
712 Klein, C., Umaña, P., and Mössner, E. (2016). Novel human IgG1 and IgG4 Fc-engineered

713 antibodies with completely abolished immune effector functions. Protein Eng Des Sel *29*,
714 457–466. https://doi.org/10.1093/protein/gzw040.

715 31. Scott, C.A.P., Amarilla, A.A., Bibby, S., Newton, N.D., Hall, R.A., Hobson-Peters, J., Muller, D.A.,
716 Chappell, K.J., Young, P.R., Modhiran, N., et al. (2021). Implications of Dengue Virus Maturation
717 on Vaccine Induced Humoral Immunity in Mice. Viruses *13*.
718 https://doi.org/10.3390/v13091843.

719 32. Newton, N.D., Hardy, J.M., Modhiran, N., Hugo, L.E., Amarilla, A.A., Bibby, S., Venugopal, H.,
720 Harrison, J.J., Traves, R.J., Hall, R.A., et al. (2021). The structure of an infectious immature
721 flavivirus redefines viral architecture and maturation. Science Advances *7*, eabe4507.
722 https://doi.org/10.1126/sciadv.abe4507.

723 33. Djender, S., Beugnet, A., Schneider, A., and Marco, A.D. (2014). The Biotechnological
724 Applications of Recombinant Single-Domain Antibodies are Optimized by the C-Terminal
725 Fusion to the EPEA Sequence (C Tag). Antibodies *3*, 182–191.
726 https://doi.org/10.3390/antib3020182.

727 34. De Genst, E.J., Guilliams, T., Wellens, J., O'Day, E.M., Waudby, C.A., Meehan, S., Dumoulin, M.,
728 Hsu, S.-T.D., Cremades, N., Verschueren, K.H.G., et al. (2010). Structure and Properties of a
729 Complex of α-Synuclein and a Single-Domain Camelid Antibody. Journal of Molecular Biology
730 *402*, 326–343. https://doi.org/10.1016/j.jmb.2010.07.001.

731 35. Yonekura, K., Maki-Yonekura, S., Naitow, H., Hamaguchi, T., and Takaba, K. (2021). Machine
732 learning-based real-time object locator/evaluator for cryo-EM data collection. Commun Biol
733 *4*, 1044. https://doi.org/10.1038/s42003-021-02577-1.

734 36. Grant, T., Rohou, A., and Grigorieff, N. (2018). cisTEM, user-friendly software for single-
735 particle image processing. eLife *7*, e35383. https://doi.org/10.7554/eLife.35383.

736 37. Jung, J., Grant, T., Thomas, D.R., Diehnelt, C.W., Grigorieff, N., and Joshua-Tor, L. (2019). High-
737 resolution cryo-EM structures of outbreak strain human norovirus shells reveal size
738 variations. Proceedings of the National Academy of Sciences *116*, 12828–12832.
739 https://doi.org/10.1073/pnas.1903562116.

740 38. Croll, T.I. (2018). ISOLDE: a physically realistic environment for model building into low-
741 resolution electron-density maps. Acta Cryst D *74*, 519–530.
742 https://doi.org/10.1107/S2059798318002425.

743 39. Emsley, P., Lohkamp, B., Scott, W.G., and Cowtan, K. (2010). Features and development of Coot.
744 Acta Cryst D *66*, 486–501. https://doi.org/10.1107/S0907444910007493.

745 40. Afonine, P.V., Poon, B.K., Read, R.J., Sobolev, O.V., Terwilliger, T.C., Urzhumtsev, A., and Adams,
746 P.D. (2018). Real-space refinement in PHENIX for cryo-EM and crystallography. Acta Cryst D
747 *74*, 531–544. https://doi.org/10.1107/S2059798318006551.

748 41. Lefranc, M.-P., Giudicelli, V., Ginestoux, C., Jabado-Michaloud, J., Folch, G., Bellahcene, F., Wu, Y.,
749 Gemrot, E., Brochet, X., Lane, J., et al. (2009). IMGT, the international ImMunoGeneTics
750 information system. Nucleic Acids Res. *37*, D1006-1012.
751 https://doi.org/10.1093/nar/gkn838.

752 42. Giudicelli, V., Brochet, X., and Lefranc, M.-P. (2011). IMGT/V-QUEST: IMGT standardized
753 analysis of the immunoglobulin (IG) and T cell receptor (TR) nucleotide sequences. Cold
754 Spring Harb Protoc *2011*, 695–715. https://doi.org/10.1101/pdb.prot5633.

755 43. Katoh, K., Rozewicki, J., and Yamada, K.D. (2019). MAFFT online service: multiple sequence
756 alignment, interactive sequence choice and visualization. Brief Bioinform *20*, 1160–1166.
757 https://doi.org/10.1093/bib/bbx108.

758 44. Kuraku, S., Zmasek, C.M., Nishimura, O., and Katoh, K. (2013). aLeaves facilitates on-demand
759 exploration of metazoan gene family trees on MAFFT sequence alignment server with
760 enhanced interactivity. Nucleic Acids Res *41*, W22–W28.
761 https://doi.org/10.1093/nar/gkt389.

762

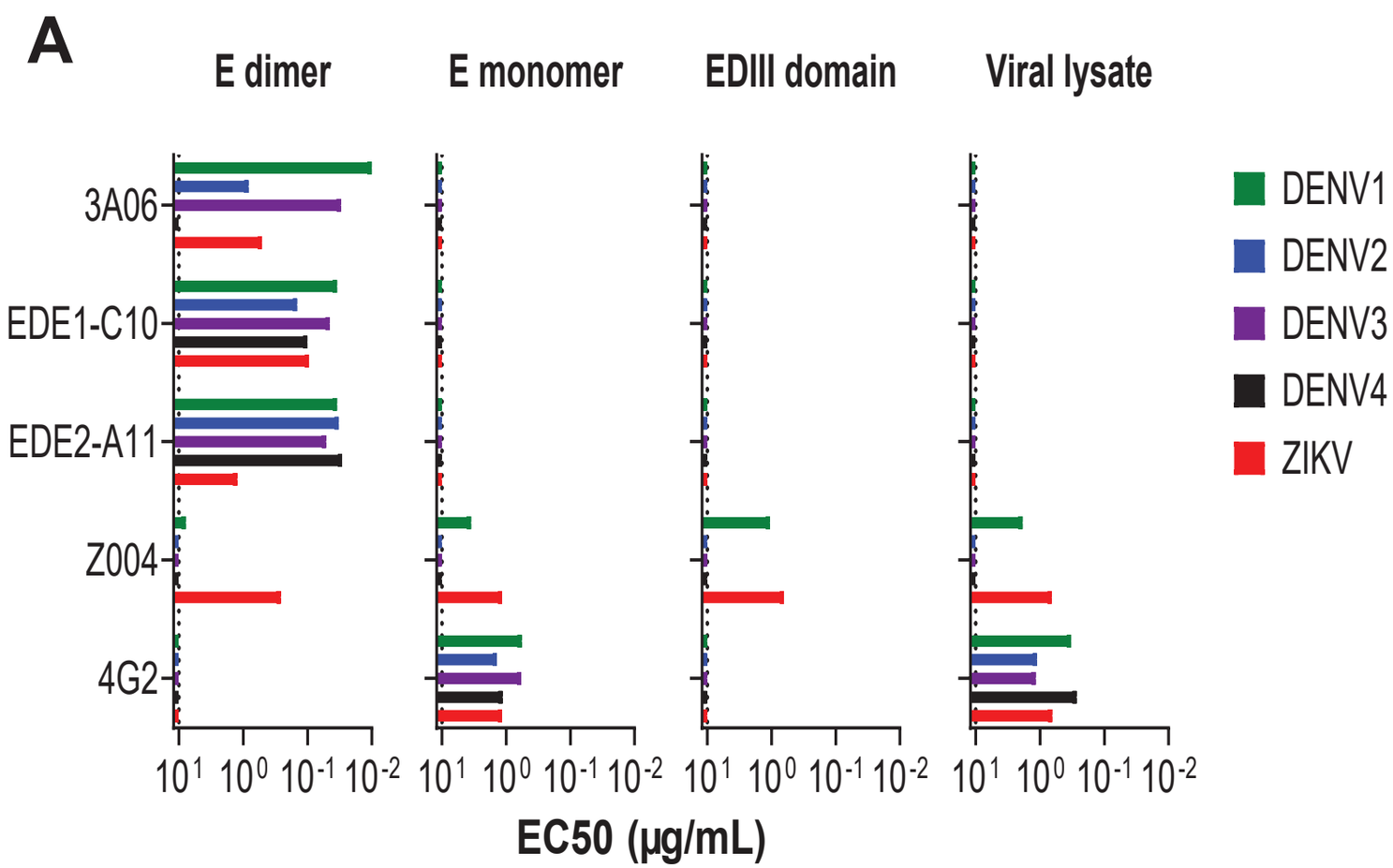

B

mAb ID	DENV1 WP74	DENV2 16681	DENV3 3001	DENV4 SL92	ZIKV PRVABC59
3A06	0.07	0.1	0.1	>20	0.3
EDE1-C10	0.3	0.3	0.6	0.07	0.1
EDE2-A11	0.6	0.6	0.6	1.25	>20

IC50 values (µg/ml)	<0.1	0.1 - 1	1 - 10.0	10.0 - 20.0	>20

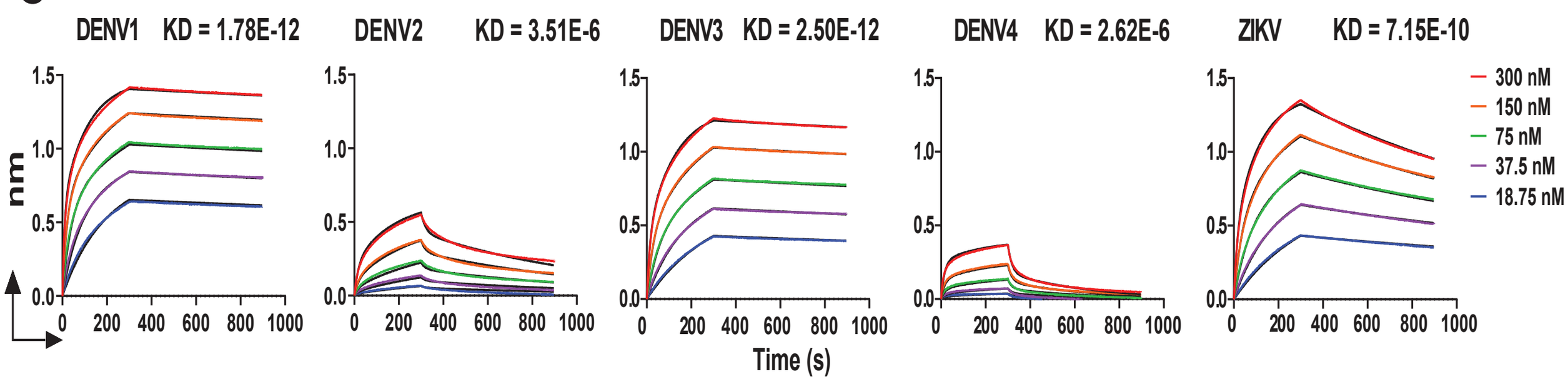

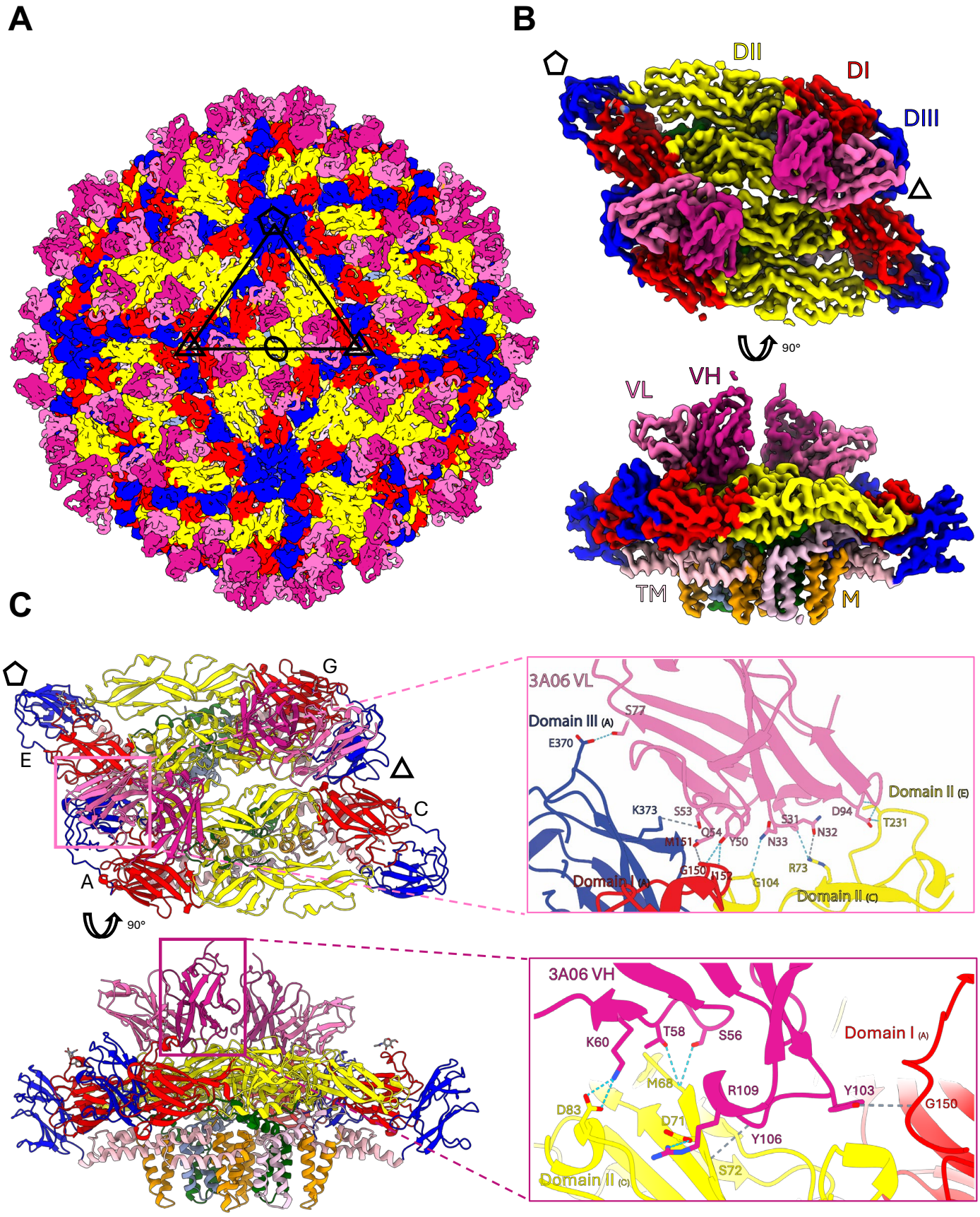
A
B
DII
DI
DIII
90°
VH
VL
TM
M
C
G
E
C
A
90°
3A06 VL
Domain III (A)
S77
E370
Domain II (E)
K373
S53
S31
D94
T231
Q54
N32
M151
Y50
N33
R73
G150
N152
G104
Domain I (A)
Domain II (C)
3A06 VH
T58
S56
K60
Domain I (A)
M68
R109
Y103
G150
D83
D71
Y106
S72
Domain II (C)

A

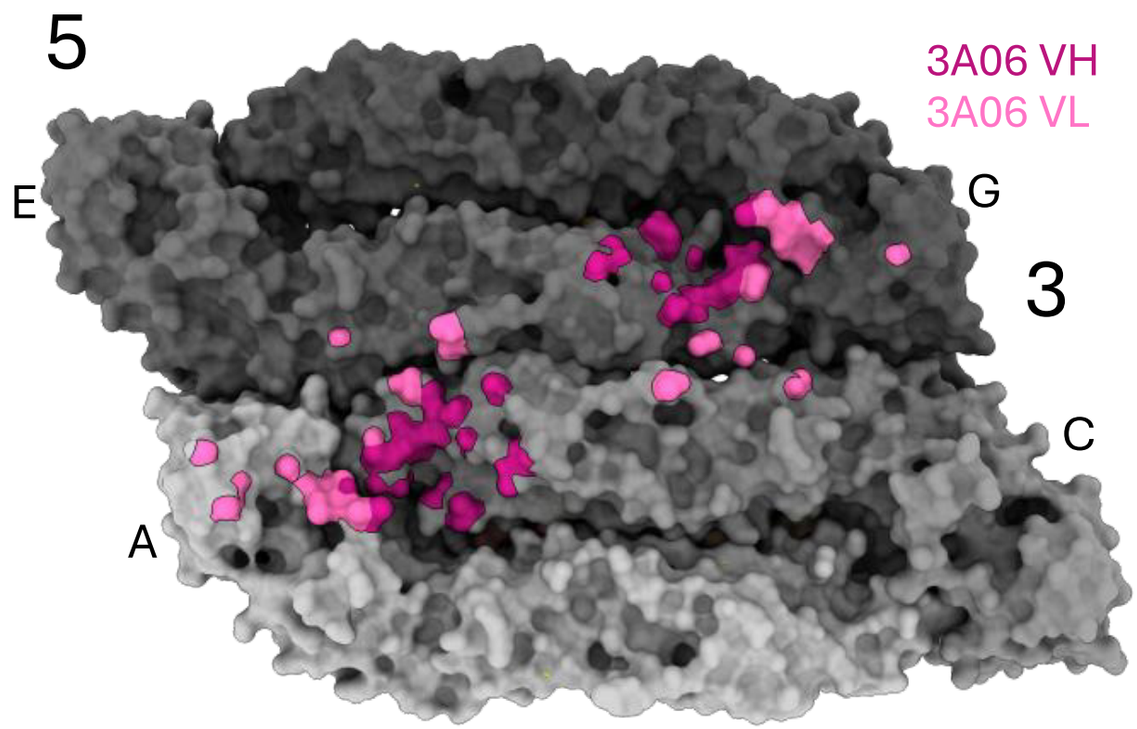
5
3A06 VH
3A06 VL
E
G
3
C
A

B

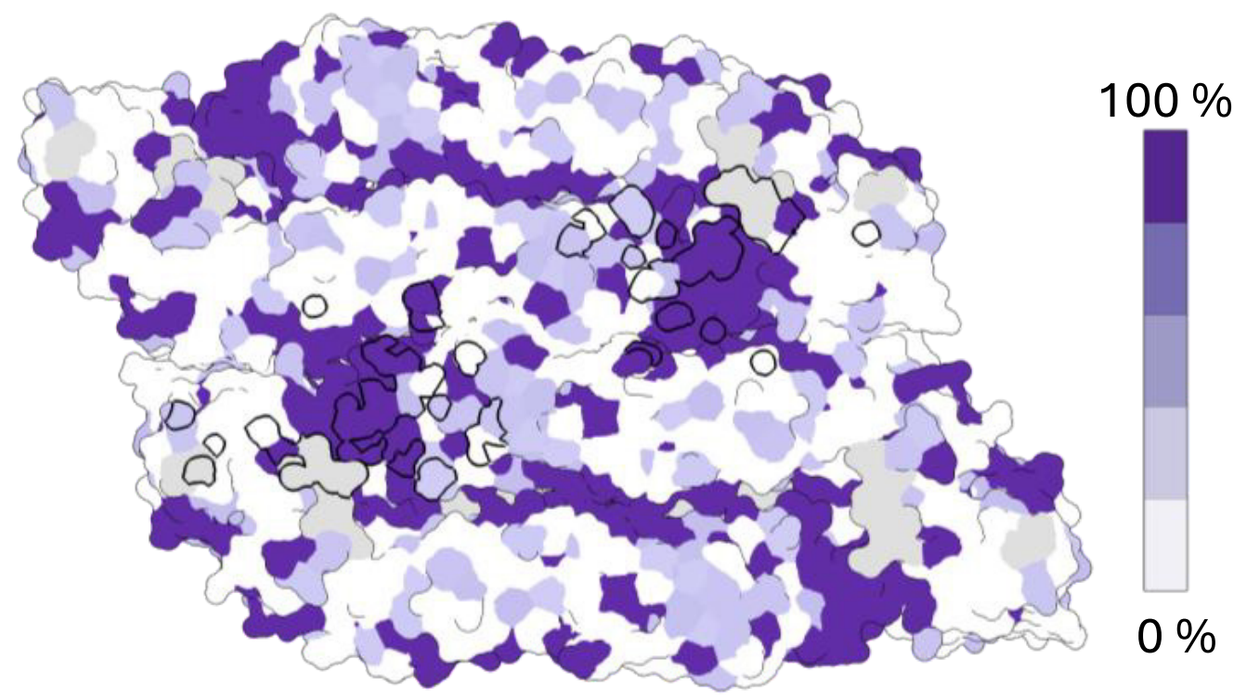
100 %
0 %

C

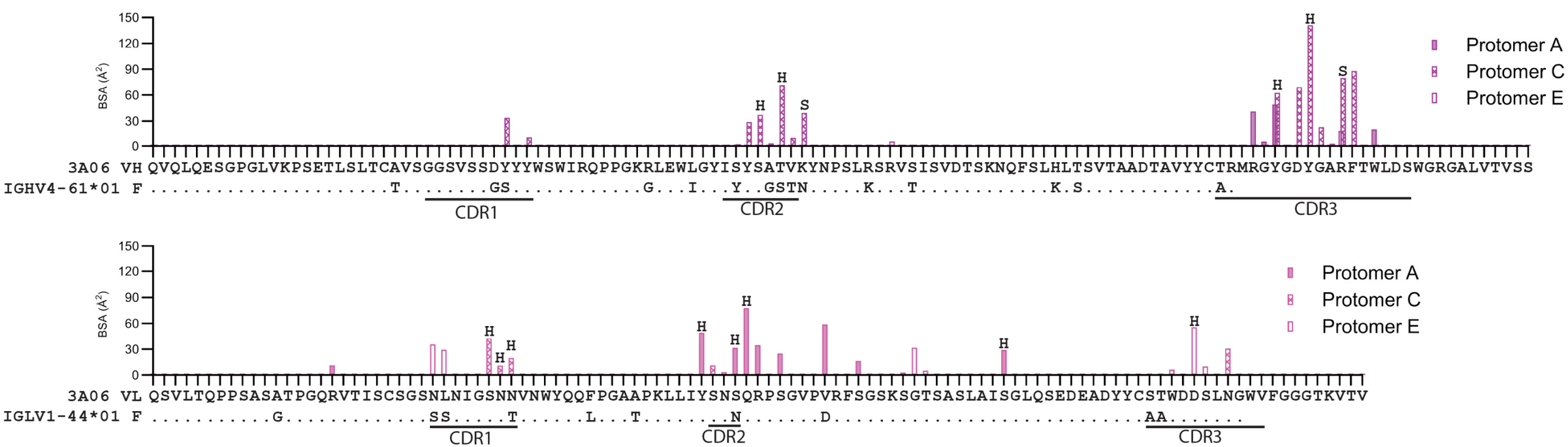
BSA (Å²)
150
120
90
60
30
0
Protomer A
Protomer C
Protomer E
3A06 VH QVQLQESGPGLVKPSETLSLTCAVSGGSVSSDYYYWSWIRQPPGKRLEWLGYISYSATVKYNPSLRSRVSISVDTSKNQFSLHLTSVTAADTAVYYCTRMRGYGDYGARFTWLDSWGRGALVTVSS
IGHV4-61*01 F .....T.....GS.....G...I...Y..GSTN.....K...T.....K.S.....A.
CDR1
CDR2
CDR3
BSA (Å²)
150
120
90
60
30
0
Protomer A
Protomer C
Protomer E
3A06 VL QSVLTQPPSASATPGQRVTISCSGSNLNIGSNNVNWYQQFPGAAPKLLIYSNSQRPSGVPVRFSGSKSGTSASLAISGLQSEDEADYYCSTWDDSLNGWVFGGGTKVTV
IGLV1-44*01 F .....G.....SS.....T.....L...T.....N.....D.....AA.....
CDR1
CDR2
CDR3

A

Somatic hypermutations reverted variants of 3A06

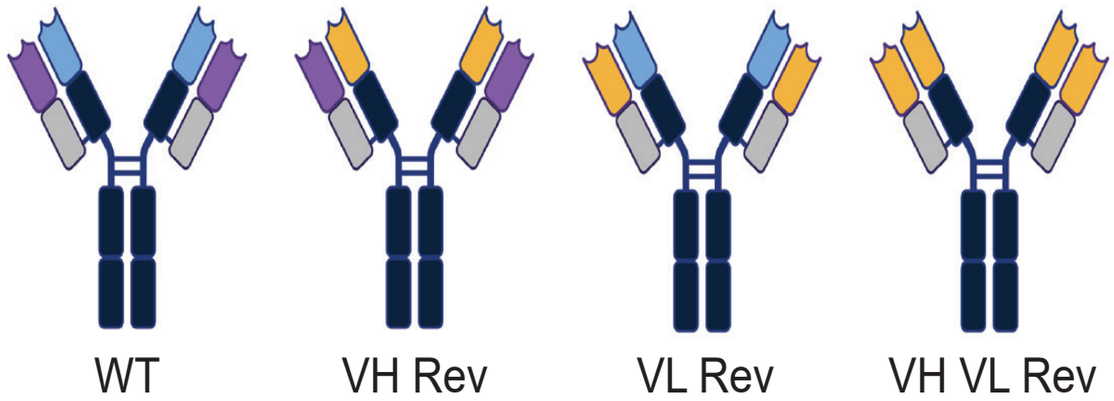

B

Improbable mutations reverted variants of 3A06

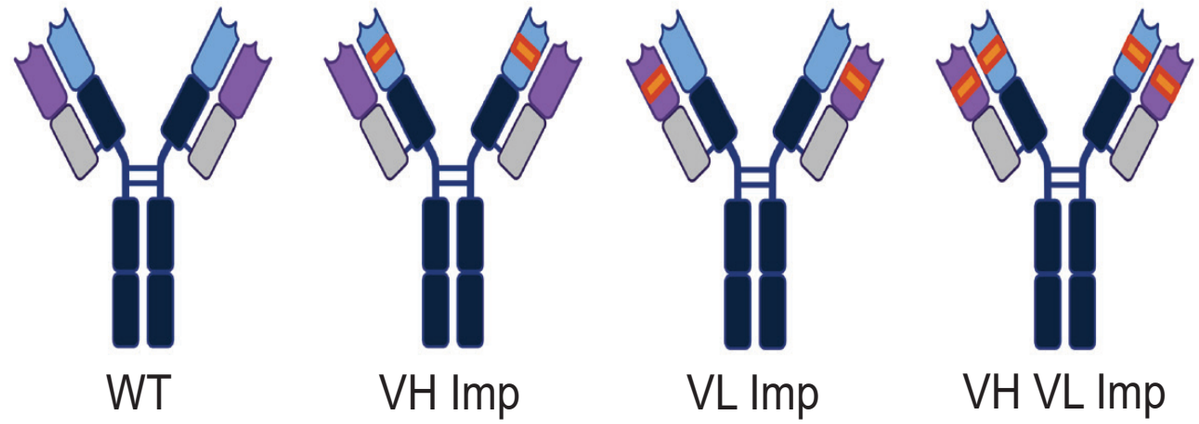

C

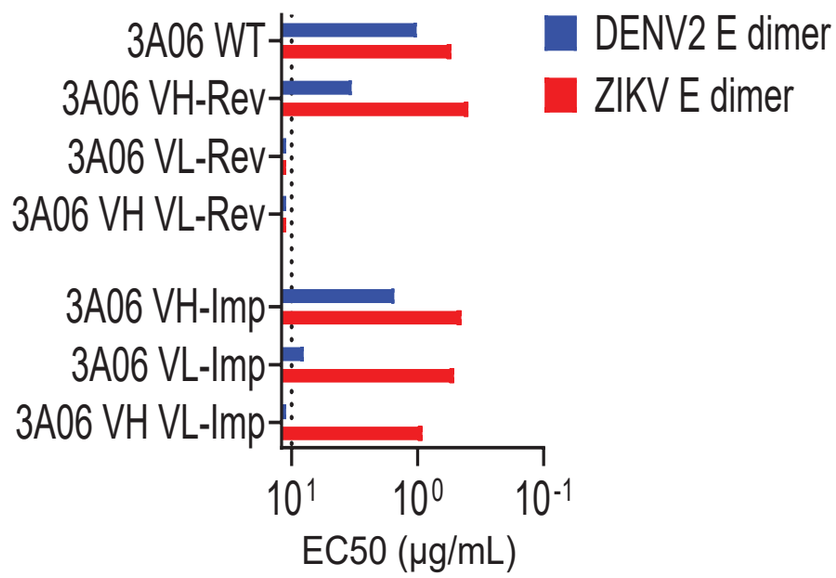

D

Antibody	DENV2 16681	ZIKV PRVABC59
3A06 WT	0.1	0.03
3A06 VH-Rev	0.6	0.07
3A06 VL-Rev	>20	>20
3A06 VH VL-Rev	>20	>20
3A06 VH-Imp	1.25	0.07
3A06 VL-Imp	10.5	2.5
3A06 VH VL-Imp	>20	2.5

IC50 values (µg/ml)
<0.1
0.1 - 1
1 - 10.0
10.0 - 20.0
>20

E

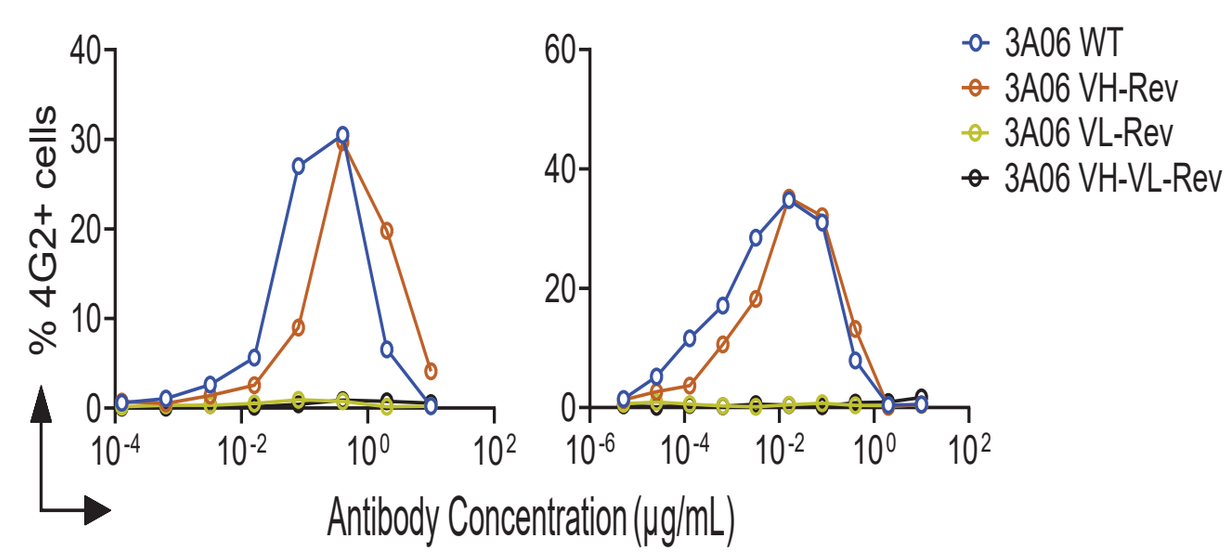

F

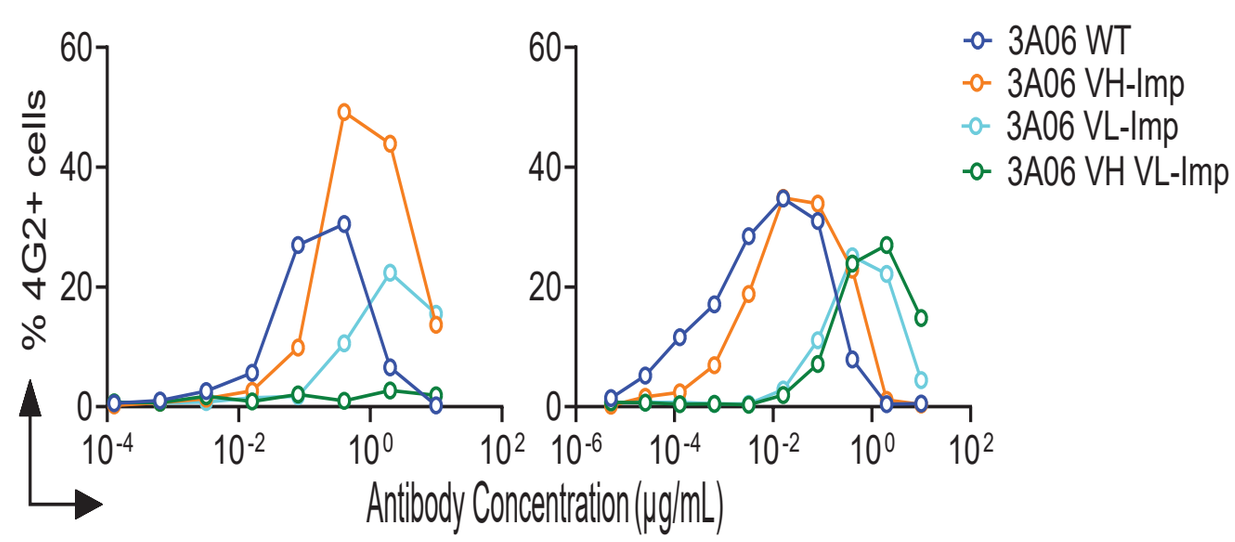

A

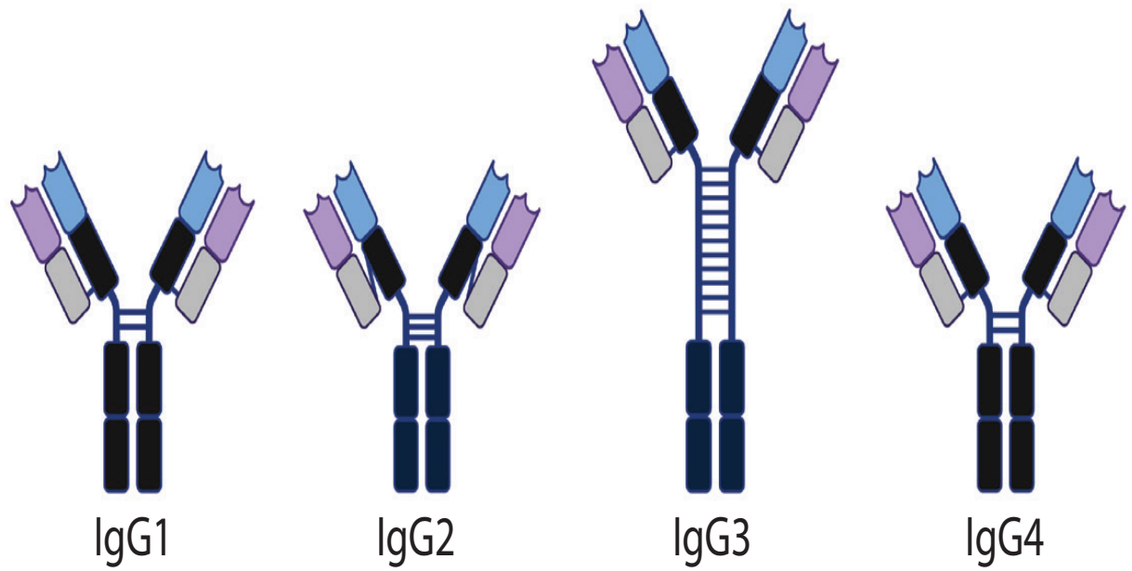

B

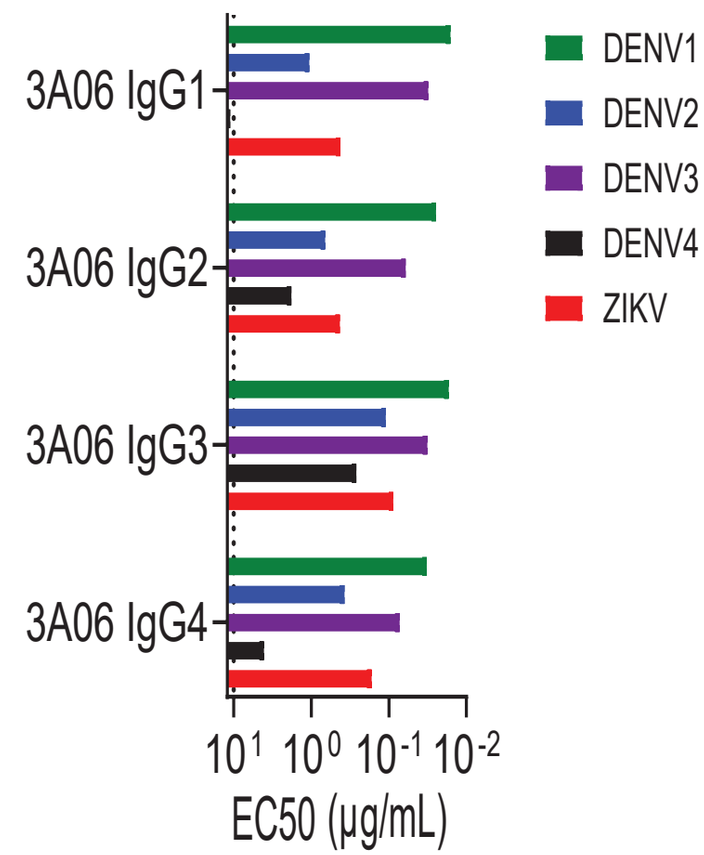

C

mAb ID	DENV1 WP74	DENV2 16681	DENV3 3001	DENV4 SL92	ZIKV PRVABC59
3A06 IgG1	0.07	0.1	0.1	>20	0.3
3A06 IgG2	0.07	0.1	0.1	10	0.6
3A06 IgG3	0.07	0.1	0.1	1.25	0.3
3A06 IgG4	0.07	0.1	0.1	10	0.3
3A06 IgG1 LALA-PG	0.07	0.1	0.1	>20	0.3
3A06 IgG3 LALA-PG	0.07	0.1	0.1	1.25	0.3

IC50 values (µg/ml)	<0.1	0.1 - 1	1 - 10.0	10.0 - 20.0	>20

D

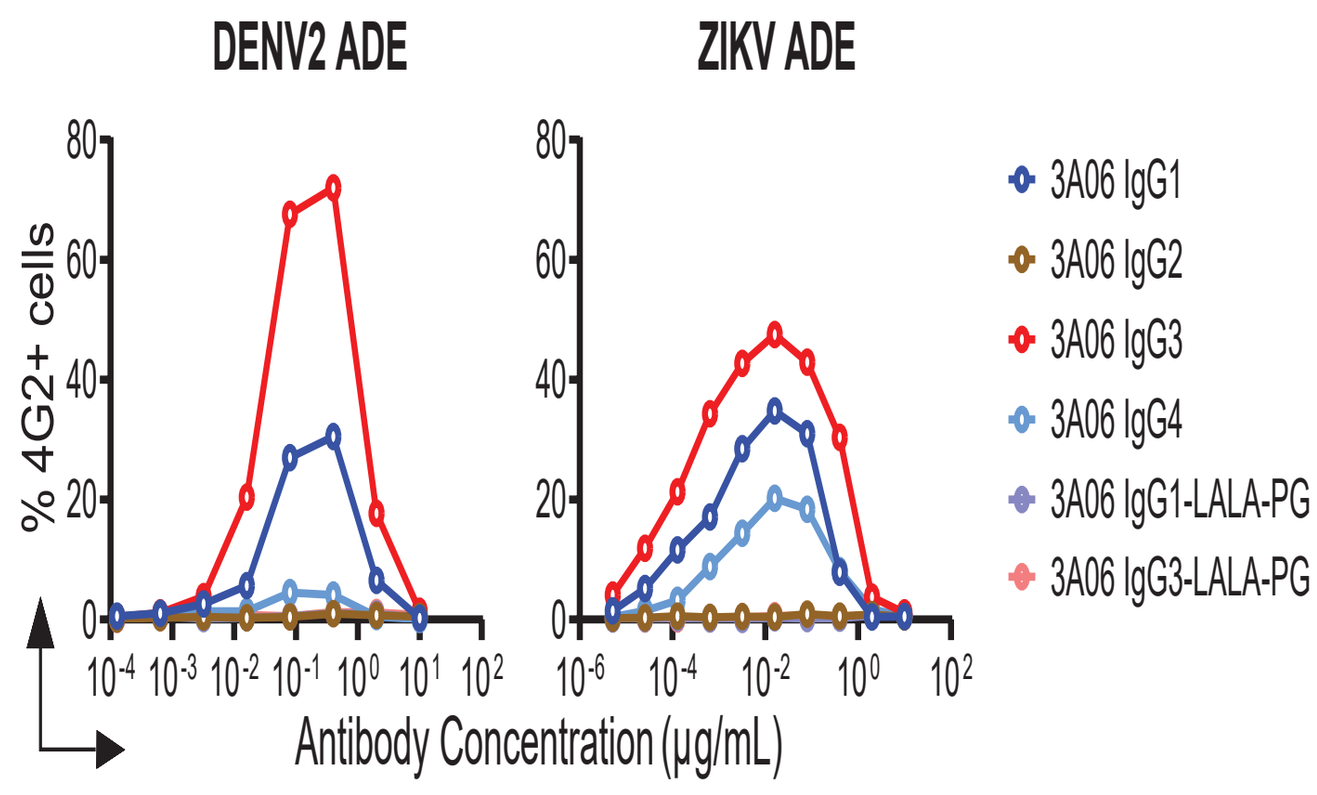

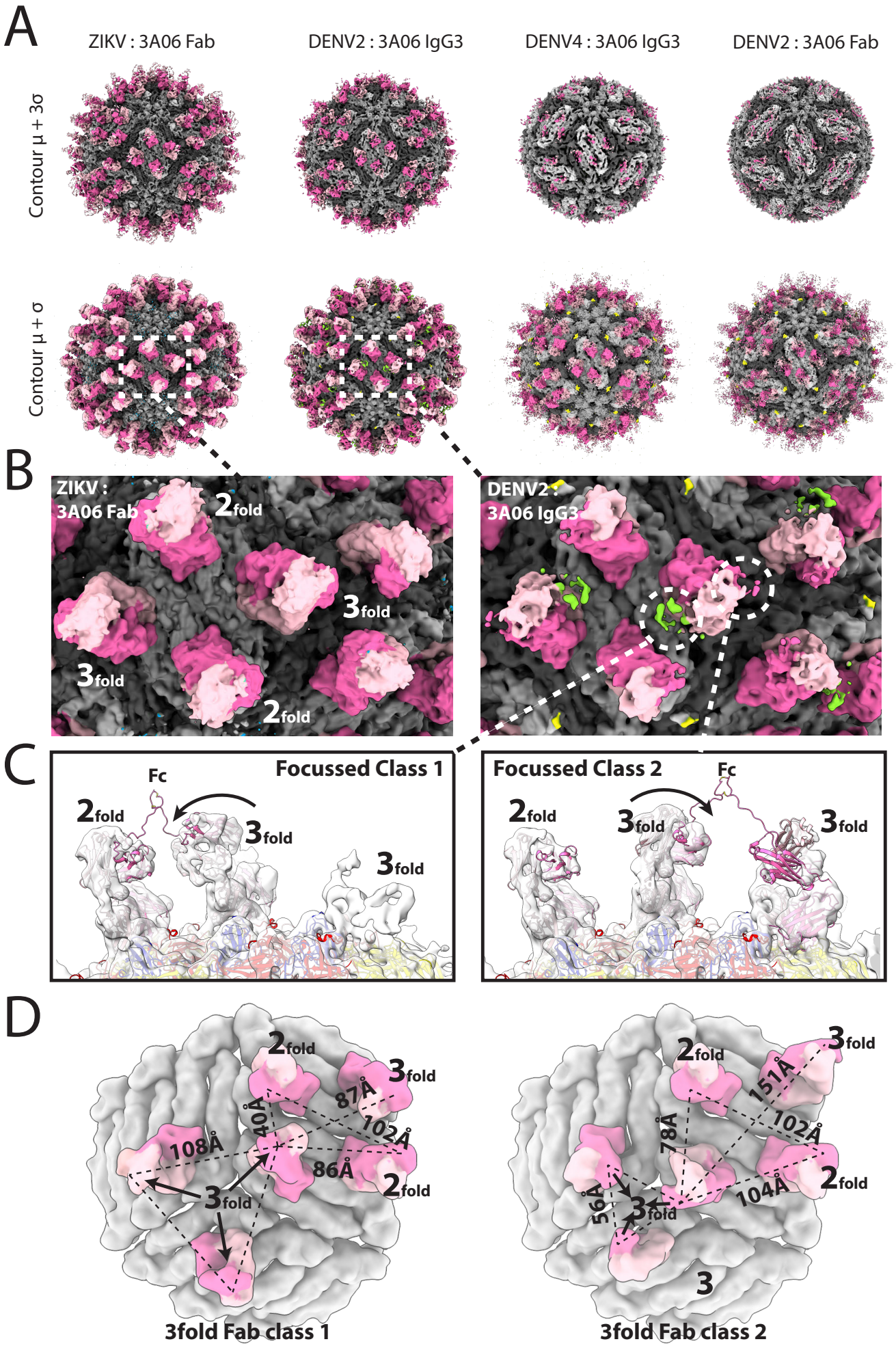
A
ZIKV : 3A06 Fab
DENV2 : 3A06 IgG3
DENV4 : 3A06 IgG3
DENV2 : 3A06 Fab
Contour μ + 3σ
Contour μ + σ
B
ZIKV :
3A06 Fab
2fold
3fold
3fold
2fold
DENV2 :
3A06 IgG3
C
Focussed Class 1
Fc
2fold
3fold
3fold
Focussed Class 2
Fc
2fold
3fold
3fold
D
2fold
3fold
87Å
40Å
102Å
108Å
86Å
2fold
3fold
3fold Fab class 1
2fold
3fold
151Å
78Å
102Å
2fold
104Å
56Å
3fold
3
3fold Fab class 2

Table 1: Comparison of immunogenetic features of quaternary E-protein epitope targeting antibodies to 3A06.

		Heavy Chain V-gene					Light Chain V-gene			
Epitope	mAb ID	V-gene	D-gene	J-gene	SHM%	CDRH3 sequence	V-gene	J-gene	SHM%	CDRL3 sequence
	33.3A06	IGHV4-61*01	IGHD4-17*01	IGHJ5*01	11.34	TRMRGYGDYGARFTWLDS	IGLV1-44*01	IGLJ3*02	6.32	STWDDSLNGWV
EDE1	**EDE1-C8**	IGHV3-64D*06	IGHD2-21*01	IGHJ6*02	6.94	VGGYSNFYYYYTMDV	IGKV3-11*01	IGKJ2*01	5.02	QQRYNWPPYT
	EDE1-C10	IGHV1-3*01	IGHD4-17*01	IGHJ4*02	2.78	ARDKVDDYGDYWFPTLWYFDY	IGLV2-14*01	IGLJ3*02	3.82	SSHTSRGTWV
EDE2	**EDE2-B7**	IGHV3-74*01	IGHD3-22*01	IGHJ6*02	6.94	ARDGVRYYYDSTGYYPDNFFQYGLDV	IGLV2-23*01	IGLJ3*02	4.51	CSYAGGKSLV
	EDE2-A11	IGHV3-74*01	IGHD3-22*01	IGHJ6*02	8.68	VRDGVRFYYDSTGYYPDSFFKYGMDV	IGLV2-23*01	IGLJ3*02	6.94	CSYATSRTLV
Quaternary	**SIgN-3C**	IGHV1-46*01	IGHD3-22*01	IGHJ5*01	12.4	ARGGRALFYDSYTTPRDGGSWWFDP	IGKV1-33*01	IGKJ5	8.51	QQFDDLPIT